Exh. 11

Interaction Notes

Note 236

August 1974

Transient Scattering by a Thin Wire in Free Space and above Ground Plane Using the Singularity Expansion Method

K. R. Umashankar

and

D. R. Wilton
University of Mississippi
University, Mississippi

Abstract

A thin straight wire is characterized in both free space and above a conducting ground plane using the singularity expansion method. Based on matrix and numerical methods the natural resonant frequencies, modal current distributions, transient and steady state reponses are given. Some of the anomalous behavior of the structure over the ground plane is discussed.

SECTION I

1.1 Brief review and matrix formulation of SEM

Consider a perfectly conducting scatterer in a linear homogeneous isotropic medium as shown in Figure 1. Assuming an e^{st} time dependence, the scattered electric field $\vec{E}^{sca}(\vec{r},s)$ at any point P can be written in terms of the induced surface current distribution $\vec{J}(\vec{r},s)$ on the object with boundary $\sum$ as [1]

$$\vec{E}^{sca} = \frac{-j\omega}{k^2}[k^2\vec{A} + \nabla(\nabla\cdot\vec{A})] \tag{1.1}$$

and

$$\vec{A} = \frac{\mu}{4\pi}\int_{\sum} \vec{J}\,\frac{e^{-jk|\vec{r}-\vec{r}'|}}{|\vec{r}-\vec{r}'|}\,d\sigma' \tag{1.2}$$

where $\vec{r}$ and $\vec{r}'$ are space vectors denoting the field point and source point variables and $\vec{A}$ is the magnetic vector potential. Hence, by substituting (1.2) into (1.1),

$$\vec{E}^{sca}(\vec{r},s) = \frac{1}{s\varepsilon}\left[\frac{-s^2}{c^2} + \nabla\nabla\cdot\right]\int_{\sum} \vec{J}(\vec{r}',s)\,\frac{e^{-\frac{s}{c}|\vec{r}-\vec{r}'|}}{4\pi|\vec{r}-\vec{r}'|}\,d\sigma' \tag{1.3}$$

where the usual representation of the fields in the frequency domain as Fourier transformed quantities is interpreted instead in terms of the slightly more suitable bilateral Laplace transformed quantities. This is done simply by the change of variables $s = j\omega$, which implies that the propagation constant

$$\gamma = jk = \frac{s}{c} = \frac{\sigma}{c} + j\frac{\omega}{c} \tag{1.4}$$

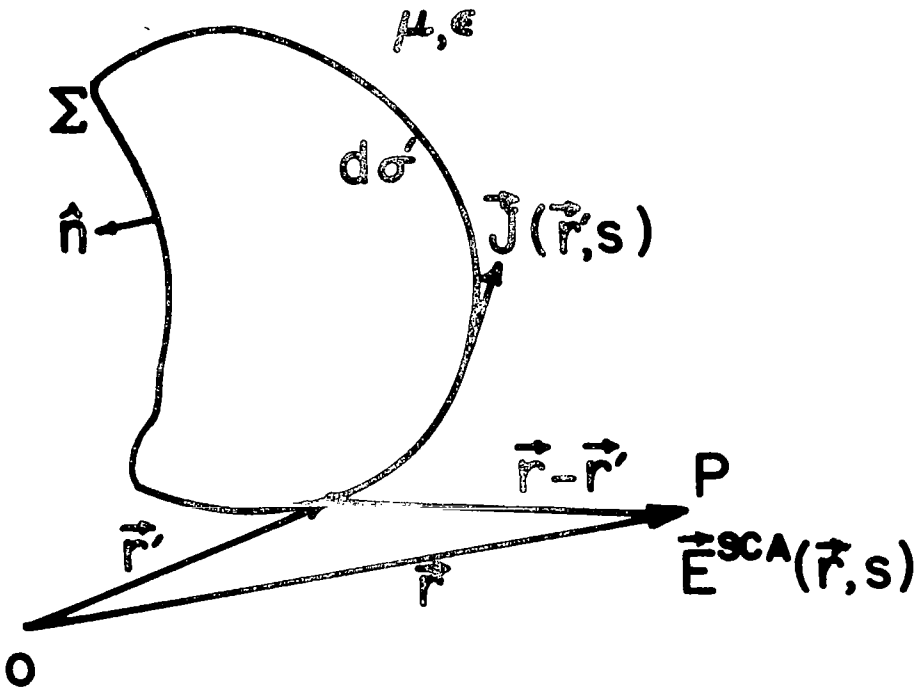

Figure 1. Perfectly conducting scatterer in a linear, homogeneous, isotropic medium.

where $c = 1/\sqrt{\mu\varepsilon}$ is the speed of light in the medium.

If $\vec{\vec{E}}^{i}(r,s)$ represents the Laplace transformed external incident field, and if we require the tangential components of the total electric field to vanish on the surface of the conducting surface $\sum$, we have

$$\hat{n} \times \left[\vec{\vec{E}}^{i}(\vec{r},s) + \vec{\vec{E}}^{sca}(\vec{r},s)\right] = 0 \tag{1.5}$$

Expressions (1.3) and (1.5) yield the following integro-differential equation for the unknown induced surface current distribution $\vec{\vec{J}}(\vec{r},s)$,

$$\hat{n} \times \left\{ \frac{-1}{s\varepsilon}\left[-\frac{s^2}{c^2} + \nabla\nabla\cdot\right] \int_{\sum} \vec{\vec{J}}(\vec{r}',s)\, \frac{e^{-\frac{s}{c}|\vec{r}-\vec{r}'|}}{4\pi|\vec{r}-\vec{r}'|}\, d\sigma' \right\}$$

$$= \hat{n} \times \vec{\vec{E}}^{i}(\vec{r},s) \tag{1.6}$$

We shall use the method of moments [2] and expand $\vec{\vec{J}}(\vec{r},s)$ in terms of a known basis set

$$\vec{\vec{J}}(\vec{r},s) = \sum_{n} I_n(s)\vec{\vec{F}}_n(\vec{r}) \tag{1.7}$$

$$n = 1,2, \ldots, N$$

where the set of vector expansion functions $\vec{\vec{F}}_n(\vec{r})$ has only components tangential to the boundary surface $\sum$ and constitutes a suitable set of basis functions, and the unknowns $I_n(s)$ are the corresponding constant current coefficients which depend only on s. The expression (1.6) may

be rewritten in operator notation as

$$\hat{n} \times \mathcal{L}_o(\vec{J}) = \hat{n} \times \vec{E}^i \tag{1.8}$$

where $\mathcal{L}_o$ is a linear integro-differential operator. Substituting (1.7) into (1.8) yields the functional equation

$$\sum_n I_n[\hat{n} \times \mathcal{L}_o(\vec{F}_n)] = \hat{n} \times \vec{E}^i \tag{1.9}$$

The above functional equation is reduced to a system of linear algebraic equations by "testing" both sides of (1.9) with a set of testing functions $\vec{W}_m(\vec{r})$. A suitable inner product for the problem may now be defined for vectors with tangential components only as

$$\langle \vec{P}, \vec{Q} \rangle = \int_{\Sigma} \vec{P} \cdot \vec{Q} \, d\sigma' \tag{1.10}$$

The method of moments then requires that

$$\sum_n I_n \langle \vec{W}_m, \hat{n} \times \mathcal{L}_o(\vec{F}_n) \rangle = \langle \vec{W}_m, \hat{n} \times \vec{E}^i \rangle$$

$$m = 1,2, \ldots, N \tag{1.11}$$

which in matrix notation forms a linear system of equations

$$\bar{\bar{Z}}(s)\bar{I}(s) = \bar{V}(s) \tag{1.12}$$

where

$$\bar{I}(s) = \begin{bmatrix} I_1(s) \\ I_2(s) \\ \cdot \\ \cdot \\ \cdot \\ I_N(s) \end{bmatrix} \tag{1.13}$$

$$\bar{V}(s) = \begin{bmatrix} \langle \vec{W}_1, \hat{n} \times \vec{E}^i \rangle \\ \langle \vec{W}_2, \hat{n} \times \vec{E}^i \rangle \\ \cdot \\ \cdot \\ \cdot \\ \langle \vec{W}_N, \hat{n} \times \vec{E}^i \rangle \end{bmatrix} . \tag{1.14}$$

and

$$\bar{\bar{Z}}(s) = [Z_{mn}]$$

$$= \begin{bmatrix} \langle \vec{W}_1, \hat{n} \times \mathcal{L}_s(\vec{F}_1) \rangle & \cdots & \langle \vec{W}_1, \hat{n} \times \mathcal{L}_s(\vec{F}_N) \rangle \\ \cdot & & \cdot \\ \cdot & & \cdot \\ \cdot & & \cdot \\ \langle \vec{W}_N, \hat{n} \times \mathcal{L}_s(\vec{F}_1) \rangle & \cdots & \langle \vec{W}_N, \hat{n} \times \mathcal{L}_s(F_N) \rangle \end{bmatrix} \tag{1.15}$$

While other forms of integral equations are derivable from (1.6), the net result after the application of the moment method is a form similar to (1.12).

Both the current expansion and the number of testing functions have been truncated to some number N so that the equation (1.12) is an N x N

matrix equation for the unknown current coefficients $I_n(s)$. The notation in (1.12) is chosen to emphasize the similarity between the present problem and the similar problem of finding the port currents for an N-port network if the voltages at each port and the impedance matrix are specified. Accordingly, the matrix $\bar{\bar{Z}}(s)$ is called the "generalized impedance matrix" and $\bar{V}(s)$ and $\bar{I}(s)$ are the "generalized voltages and currents" respectively. For most of the following discussion, we may alternatively think of $\bar{\bar{Z}}$ as the integral operator of equation (1.6), $\bar{I}$ as the surface current $\bar{J}$, and $\bar{V}$ as the incident excitation $\hat{n} \times \bar{E}^i$. With this interpretation, equation (1.12) may be thought of as equation (1.6) written in operator notation. The solution of (1.12) is

$$\bar{I}(s) = \bar{\bar{Z}}^{-1}(s)\ \bar{V}(s) = \bar{\bar{Y}}(s)\ \bar{V}(s) \tag{1.16}$$

where $\bar{\bar{Y}}(s)$ is the so-called generalized admittance matrix, the inverse of the impedance matrix. The elements of $\bar{\bar{Y}}(s)$ are given by

$$\bar{\bar{Y}}(s) = [Y_{nm}(s)] = \left[\frac{(-1)^{m+n}\ \Delta_{mn}(s)}{\Delta(s)}\right] \tag{1.17}$$

where $\Delta_{mn}(s)$ is a minor determinant of $\bar{\bar{Z}}(s)$ formed by deleting the m-th row and the n-th column, and $\Delta(s)$ is the determinant of $\bar{\bar{Z}}(s)$.

Examining the analytic properties of the various quantities in (1.17) in the complex s-plane, we observe that every element of the matrix $\bar{\bar{Z}}(s)$ in (1.15) is analytic throughout the finite complex s-plane

except for a possible pole singularity at $s = 0$. Because the quantities $\Delta_{mn}(s)$ and $\Delta(s)$ are found by taking product factors of all the elements in $\bar{\bar{Z}}(s)$ they are also analytic everywhere except possibly at $s = 0$. Hence the only possible singularities of $\bar{\bar{Y}}(s)$ are the zeros of $\Delta(s)$ (and at $s = 0$) which are therefore poles of $\bar{\bar{Y}}(s)$.

We now write (1.16) in a partial fraction expansion

$$\bar{I}(s) = \sum_i \frac{\bar{\bar{Y}}_i^r}{s-s_i} \bar{V}(s) + \bar{W}_e(s) \tag{1.18}$$

In equation (1.18), the singularities of $\bar{\bar{Y}}(s)$ are located at $s = s_i$ and $\bar{\bar{Y}}_i^r$ denotes the corresponding matrix of residues of $\bar{\bar{Y}}(s)$, given by

$$\bar{\bar{Y}}_i^r = \lim_{s \to s_i} [(s-s_i)\bar{\bar{Y}}(s)] \tag{1.19}$$

and $\bar{W}_e(s)$ is a column vector whose elements are entire functions, i.e., it has singularities only at infinity. For convenience in notation, it is assumed here that all poles are of first order, as always appears to be the case for perfectly conducting objects. If higher order poles are present the above development must be modified accordingly. We will also drop the term $\bar{W}_e(s)$, assuming it to be zero. This has been found to be the case in a number of exactly solvable geometries, but it has not yet been shown to be true in general. We will take the point of view that the singularities at infinity, if they do exist, seem to have negligible effect on numerical results. Hence, the expression (1.18) becomes

$$\bar{I}(s) = \sum_i \frac{\bar{\bar{Y}}_i^r}{s-s_i} \bar{V}(s) \tag{1.20}$$

It is possible to further simplify the expression (1.20) to a form that is very compact and convenient for numerical computation. At the so-called natural resonant frequencies, $s = s_i$, there exist non-trivial solutions $\overline{I}_i$ to the homogeneous problems

$$\overline{\overline{Z}}_i \overline{I}_i = \overline{0} \tag{1.21}$$

where $\overline{\overline{Z}}_i = \overline{\overline{Z}}(s_i)$. There also exist non-trivial solutions to the homogeneous adjoint problem

$$\left.\begin{aligned} \overline{\overline{Z}}_i^T \overline{H}_i^* &= \overline{0} \\ \text{or} \qquad \overline{\overline{Z}}_i^\dagger \overline{H}_i &= \overline{0} \end{aligned}\right\} \tag{1.22}$$

where T denotes the transpose, the asterisk denotes complex conjugate, and the dagger denotes complex conjugate transpose or adjoint. In order for (1.21) and (1.22) to hold, the determinant

$$\Delta(s) = |\overline{\overline{Z}}(s)| \tag{1.23}$$

must vanish at $s = s_i$. We will assume for convenience in the following that $\Delta(s)$ has only simple zeros and that there is only one set of solution vectors $\overline{I}_i$ and $\overline{H}_i$ of equations (1.21) and (1.22) respectively. The extension to the more general case where $\Delta(s)$ has multiple zeros or when (1.21) and (1.22) have a degenerate set of solutions is relatively straightforward but introduces uninteresting notational complications in the development.

We may write the solution of (1.12) in several equivalent forms:

$$\bar{I}(s) = \bar{\bar{Z}}^{-1}(s)\,\bar{V}(s) = \bar{\bar{Y}}(s)\,\bar{V}(s) = \sum_i \frac{\bar{\bar{Y}}_i^r}{s-s_i}\,\bar{V}(s) \tag{1.24}$$

Since we assumed that $\Delta(s)$ has only simple zeros, $\bar{\bar{Y}}(s)$ has only simple poles. The elements of $\bar{\bar{Y}}(s)$ are all meromorphic functions of the complex frequency variable and the numerical methods discussed in Appendix A may be used to evaluate the residue matrix $\bar{\bar{Y}}_i^r$.

If it were necessary to use the form of the singularity expansion of $\bar{I}(s)$ given in (1.24), SEM would be somewhat impractical for numerical computation because the residue matrix $\bar{\bar{Y}}_i^r$ would have to be stored for each resonant frequency. For most practical problems, this requirement could quickly use up all available machine storage. Fortunately, it can be shown that $\bar{\bar{Y}}_i^r$ is a dyadic; that is, its elements can be calculated as the product of elements taken from two column vectors. One of these column vectors is just the modal current $\bar{I}_i$ of equation (1.21). To show this we note that

$$\bar{\bar{Z}}(s)\,\bar{\bar{Y}}(s) = \bar{\bar{Y}}(s)\,\bar{\bar{Z}}(s) = \bar{\bar{U}}$$

$$= \sum_i \frac{\bar{\bar{Z}}(s)\,\bar{\bar{Y}}_i^r}{s-s_i} = \sum_i \frac{\bar{\bar{Y}}_i^r \bar{\bar{Z}}(s)}{s-s_i}$$

where $\bar{\bar{U}}$ is the identity matrix. Hence

$$\lim_{s\to s_i} (s-s_i)\,\bar{\bar{Z}}(s)\,\bar{\bar{Y}}(s) = \lim_{s\to s_i} (s-s_i)\,\bar{\bar{Y}}(s)\,\bar{\bar{Z}}(s)$$

$$= \lim_{s\to s_i} (s-s_i)\,\bar{\bar{U}}$$

$$= \bar{Z}_i \bar{Y}_i^r = \bar{Y}_i^r \bar{Z}_i = \bar{0}$$

or equivalently,

$$\bar{Z}_i \bar{Y}_i^r = \bar{0}$$

and

$$\bar{Z}_i^\dagger \bar{Y}_i^{r\dagger} = \bar{0} \tag{1.25}$$

Comparison of (1.25) with (1.21) shows that the columns of $\bar{Y}_i^r$ must be proportional to $\bar{I}_i$ and the rows must be proportional to $\bar{H}_i^\dagger$. Hence $\bar{Y}_i^r$ can be written in the form

$$\bar{Y}_i^r = \beta_i \bar{I}_i \bar{H}_i^\dagger \tag{1.26}$$

where β_i is a constant to be determined. Using (1.26), $\bar{Y}(s)$ may be expressed as

$$\bar{Y}(s) = \sum_i \beta_i \frac{\bar{I}_i \bar{H}_i^\dagger}{s-s_i} \tag{1.27}$$

To determine β_i, we note that

$$\bar{H}_j^\dagger \bar{Z}(s) \bar{Y}(s) \bar{H}_j = \bar{H}_j^\dagger \bar{U} \bar{H}_j = ||\bar{H}_j||^2 \tag{1.28}$$

where $||\bar{A}||$ denotes the norm of a vector $\bar{A}$,

$$||\bar{A}|| = \sqrt{\bar{A}^\dagger \bar{A}}$$

With (1.27) and (1.28), we have

$$\sum_i \beta_i \frac{\bar{H}_j^\dagger \bar{Z}(s) \bar{I}_i \bar{H}_i^\dagger \bar{H}_j}{s-s_i} = ||\bar{H}_j||^2$$

If we note that

$$\bar{H}_j^\dagger \bar{Z}_j \bar{I}_i = \bar{H}_j^\dagger \bar{Z}_j^{\dagger\dagger} \bar{I}_i$$

$$= (\bar{Z}_j^\dagger \bar{H}_j)^\dagger \bar{I}_i = \bar{0}$$

then we can write

$$\sum_i \beta_i \frac{\bar{H}_j^\dagger (\bar{Z}(s) - \bar{Z}_j) \bar{I}_i \bar{H}_i^\dagger \bar{H}_j}{s-s_i} = ||\bar{H}_j||^2$$

We now take the limit on the left hand side as s approaches s_j and note that

$$\lim_{s \to s_j} \frac{\bar{Z}(s) - \bar{Z}_j}{s-s_i} = \bar{Z}_j' \delta_{ij}$$

where $\bar{Z}_j'$ is the derivative

$$\left.\frac{d\bar{Z}}{ds}\right|_{s=s_j} = \bar{Z}_j'$$

and δ_{ij} is the Kronecker delta. The result is

$$\beta_j \bar{H}_j^\dagger \bar{Z}_j' \bar{I}_j ||\bar{H}_j||^2 = ||\bar{H}_j||^2$$

from which we conclude

$$\beta_i = \frac{1}{H_i^{\dagger} \bar{Z}_i^{r} I_i} \tag{1.29}$$

Hence $\bar{Y}(s)$ is given by

$$\bar{Y}(s) = \sum_i \frac{I_i H_i^{\dagger}}{H_i^{\dagger} \bar{Z}_i^{r} I_i (s-s_i)} \tag{1.30}$$

Note that since I_i and H_i are solutions to the homogeneous equations (1.21) and (1.22), they may be defined only to within an arbitrary constant. That this constant is arbitrary can be seen from the fact that these vectors appear in (1.30) in such a way that each term in the expression is independent of the choice of normalization. Therefore, from equation (1.20) and (1.26)

$$\bar{I}(s) = \sum_i \beta_i I_i H_i^{\dagger} \frac{\bar{V}(s)}{s-s_i} \tag{1.31}$$

Equation (1.31) is the most important result in SEM. We see that once the residue matrices $\bar{Y}_i^{r}$ are known along with the various poles $s = s_i$, the entire frequency response can be found by substituting $s = j\omega$. Hence from expression (1.31),

$$\bar{I}(j\omega) = \sum_i \beta_i I_i H_i^{\dagger} \frac{\bar{V}(j\omega)}{j\omega-s_i} \tag{1.32}$$

Alternatively, the time domain response is usually obtained by expanding $\bar{V}(s)$ in terms of its singularities, if any, and using the well known Laplace transform pair relationship for simple poles,

$$F(s) = \frac{1}{s-s_i} \quad , \quad f(t) = u(t)e^{s_i t} \tag{1.33}$$

where

$$F(s) = \int_{-\infty}^{+\infty} f(t)\, e^{-st}\, dt \tag{1.34}$$

is the Laplace transform of a time dependent function f(t) and u(t) is the Heaviside unit step function. We see immediately in (1.33) that the poles must be either in the left half of the s plane or on the imaginary axis in order to exclude fields which grow exponentially with time. Poles on the imaginary axis, however, correspond to undamped sinusoids which therefore do not lose energy by radiation. Hence poles on the imaginary axis of the s plane must correspond to interior resonances (cavity resonances) which do not radiate fields on the exterior of the scatterer and, furthermore, do not couple to the incident fields.

Many of the familiar results of circuit theory also apply to the problem at hand. For example, we know that in order to obtain real time responses, the poles must appear in complex conjugate pairs and their residues must be complex conjugates. Furthermore, one may interpret resonances in the frequency domain in terms of the nearness of the given frequency to a pole.

Hence for expression (1.31), the time domain solution is given by the Laplace inversion formula

$$\bar{i}(t) = \frac{1}{2\pi j} \int_{C_B} \sum_i \beta_i \bar{I}_i \bar{H}_i^{\dagger} \frac{\bar{V}(s)\, e^{st}}{s-s_i}\, ds \tag{1.35}$$

where C_B is the Bromwich contour (Figure 2) in the complex s plane.

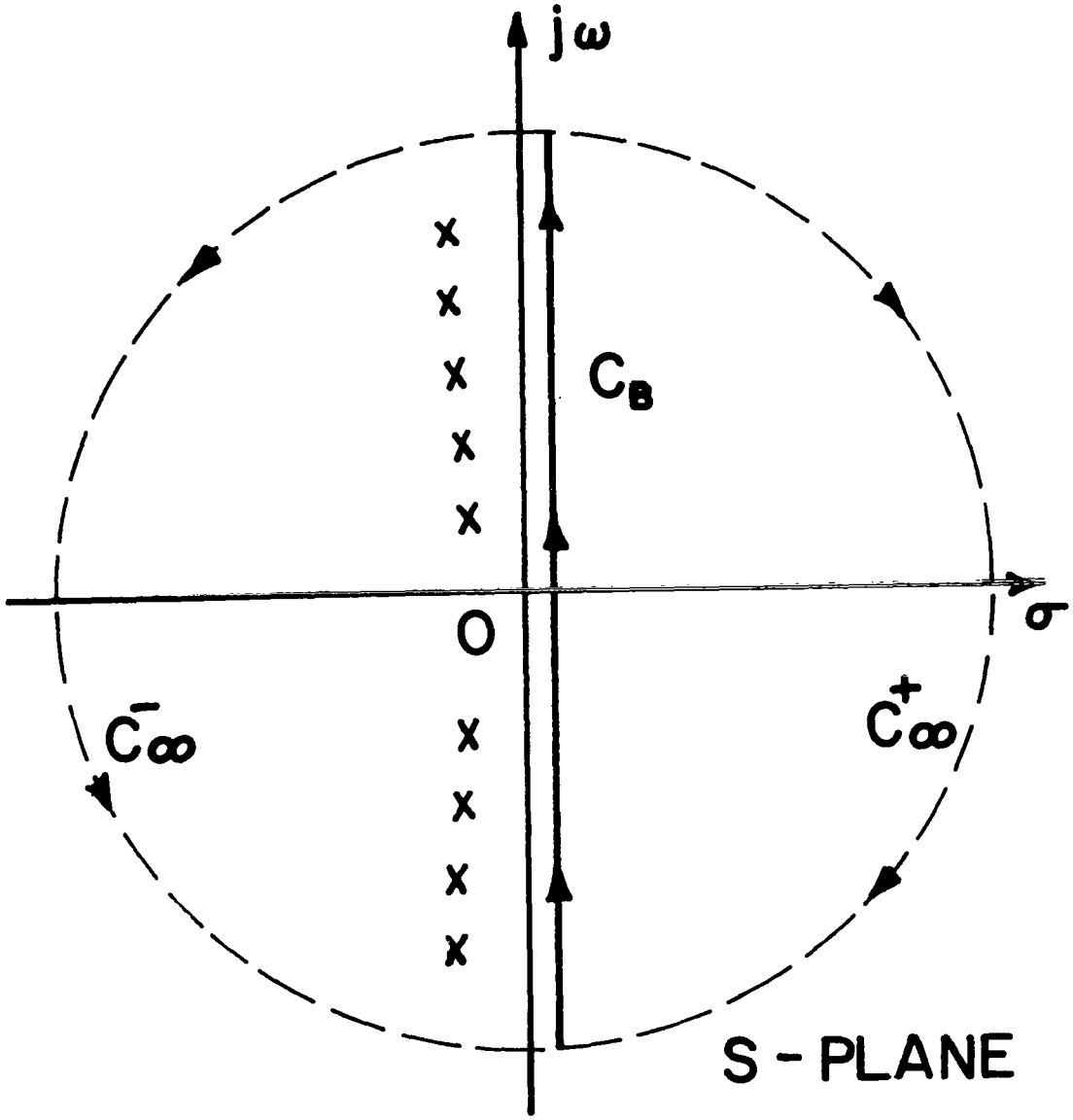

Figure 2. Illustration of the closure of the Bromwich contour in s-plane.

SECTION II

FINITE CIRCULAR CYLINDER

2-1 E-field integro-differential equation

In this section, an isolated finite circular conducting cylinder is analyzed by SEM to characterize the structure's transient scattering properties when a time varying step plane wave is incident. This problem has also been independently treated by Tesche [3] using slightly different numerical processing and showing somewhat different data than that presented here.

In Figure 3, a circular cylinder of total length L and of radius a is placed along the z axis in free space. If $E_z^i(z,s)$ is the component of the incident field along the z direction, $I_z(z,s)$ is the corresponding induced current on the surface of the conducting structure, then equation (1.6) becomes the Pocklington E-field type integro-differential equation

$$-4\pi s\varepsilon_0 E_z^i(z,s) = \left[\frac{\partial^2}{\partial z^2} - \gamma^2\right] A(z,s) \qquad (2.1)$$

where

$$A(z,s) = \int_0^L I_z(z',s)K(z,z',s)dz'$$

and where K(z,z',s) is the regular kernel function given by

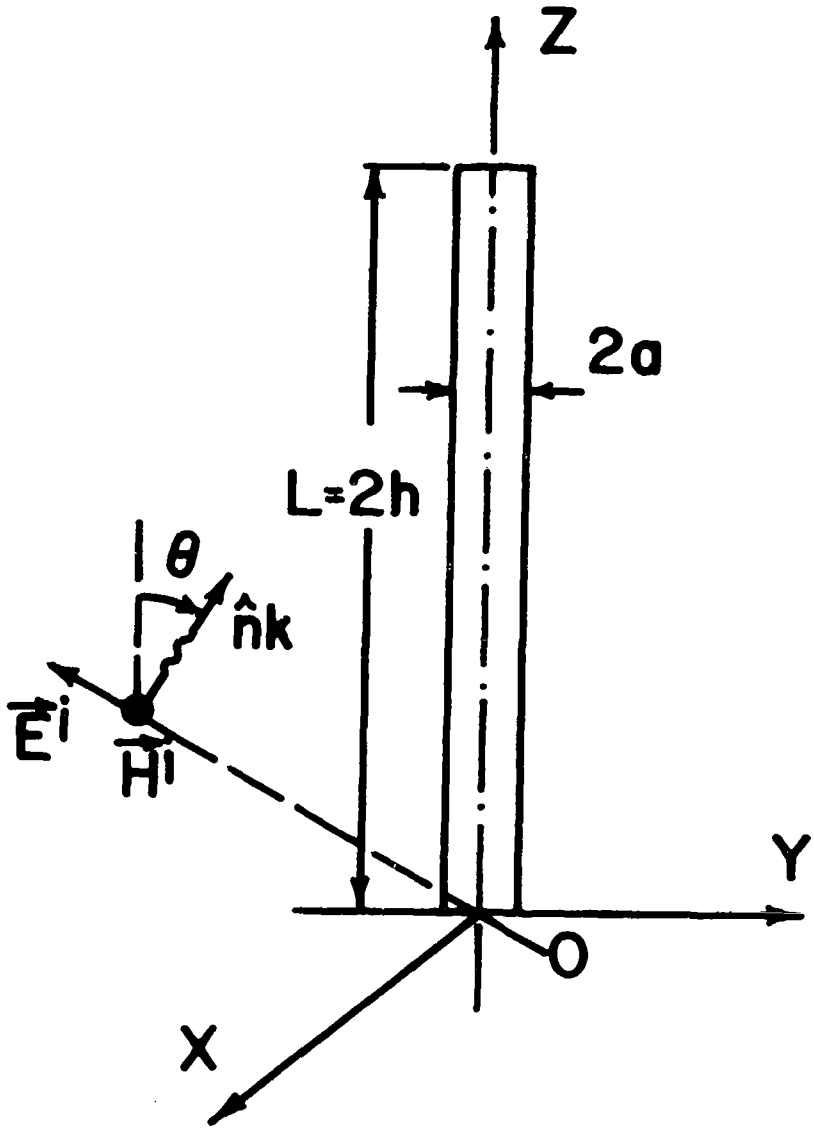

Figure 3. Geometry of isolated circular cylinder.

$$K(z,z',s) = \frac{e^{-\gamma R}}{R} \tag{2.2}$$

and

$$R^2 = a^2 + (z-z')^2 \tag{2.3}$$

$$\gamma = \frac{s}{c} \tag{2.4}$$

For E_θ-polarization, the incident electric field along the z direction is given by

$$E_z^i(z,s) = -E_0(s) \sin\theta \, e^{-\gamma \cos\theta \, z} \tag{2.5}$$

A convenient way for solving the integro-differential equation (2.1) is by the method of moments as outlined in section I, equations (1.7) to (1.11), which leads to a numerical solution for the current. The accuracy of the solution is entirely dependent on the choice of the expansion function, the testing functions and the accuracy of numerical integrations.

The integro-differential equation (2.1) is reduced to a matrix equation of the type (1.12) by dividing the structure into a number of sub-sections and expanding the unknown induced current distribution into a set of piecewise linear functions (Figure 4) over each of the sub-intervals. According to the boundary condition, the current must be zero at the ends of the structure. The resulting functional form of the expression is matched at various discrete points on the structure after approximating the differential operator by finite

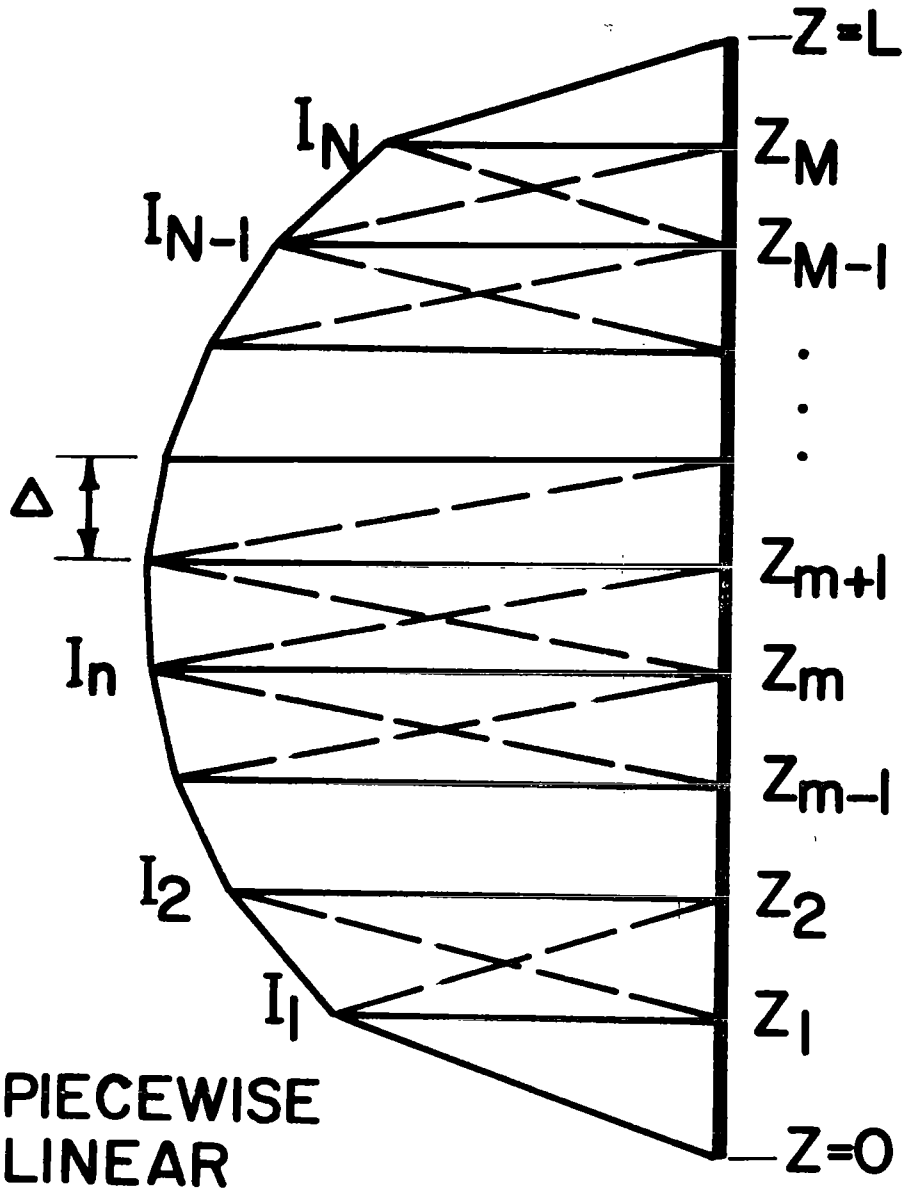

Figure 4. Piecewise linear basis set and position of match points used in the Pocklington difference-integral equation.

differences. Hence, we obtain the matrix equation

$$\bar{\bar{Z}}(s)\bar{I}(s) = \bar{V}(s) \tag{2.6a}$$

where

$$\bar{\bar{Z}}(s) = [Z_{mn}]$$

$$Z_{mn} = A(z_{m+1},s) - [\gamma^2\Delta^2+2]A(z_m,s) + A(z_{m-1},s)$$

$$A(z_m,s) = \frac{1}{\Delta}\int_{z_{n-1}}^{z_n} [z'-z_{n-1}]K(z_m,z',s)dz'$$

$$+ \frac{1}{\Delta}\int_{z_n}^{z_{n+1}} [z_{n+1}-z']K(z_m,z',s)dz'$$

$$m = 1, 2, 3, \cdots, N$$

$$n = 1, 2, 3, \cdots, N \tag{2.6b}$$

$$\bar{V}(s) = [V'_m]$$

$$V'_m = -\frac{4\pi}{\eta}\gamma\,\Delta^2\,E_0(s)\sin\theta\, e^{-\gamma\cos\theta\, z_m} \tag{2.6c}$$

$$\bar{I}(s) = \begin{vmatrix} I_1 \\ \cdot \\ \cdot \\ \cdot \\ I_N \end{vmatrix} \tag{2.6d}$$

In the above expressions, the length of the sub-section intervals is

$$\Delta = \frac{L}{N+1} \tag{2.6e}$$

and the impedance of free space is

$$\eta = [\mu_0/\epsilon_0]^{\frac{1}{2}} = 120\pi \tag{2.6f}$$

2-2 Application of SEM to the isolated circular cylinder

Every element Z_{mn} of the matrix $\overline{\overline{Z}}(s)$ defined in the expression (2.6b) is analytic throughout the finite complex plane and hence the SEM as described in chapter I, equations (1.16) to (1.20), can now be applied to the matrix equation (2.6a).

The solution for the induced current distribution on the circular cylinder is given by

$$\overline{I}(s) = \overline{\overline{Z}}^{-1}(s)\overline{V}(s)$$

and from (1.20), (1.26) and (1.31)

$$\overline{I}(s) = \sum_i \beta_i \overline{I}_i \overline{H}_i^t \frac{\overline{V}(s)}{s-s_i} \tag{2.7}$$

where $s=s_i$ are the poles or the complex natural resonant frequencies of oscillation, $\overline{I}_i$ is the modal current distribution, $\overline{H}_i$ is the coupling vector, and β_i is just a normalizing constant. The vectors $\overline{I}_i$ and $\overline{H}_i$ may be evaluated as the solution to the homogeneous equa-

tions (1.21) and (1.22). In Note 152 [8], a numerical procedure is discussed for evaluating first the residue matrix

$$\bar{\bar{Y}}_i^r = \beta_i \bar{I}_i \bar{H}_i^\dagger = \lim_{s \to s_i} (s-s_i) \bar{\bar{Z}}^{-1}(s) \tag{2.8}$$

and then the quantities $\bar{I}_i$, $\bar{H}_i$ and β_i, which are derived from the residue matrix by the methods discussed in Note 152 [8]. Because the original integral operation satisfies the reciprocity theorem, it is possible to show that in the present problem using subdomain basis and testing functions, we should have,

$$\bar{I}_i \cong \bar{H}_i^* \tag{2.9}$$

where the approximation becomes better the more accurately $\bar{I}_i$ and $\bar{H}_i$ are calculated.

The frequency domain solution corresponding to the time harmonic plane wave excitation (or the frequency response of a time domain delta function plane wave excitation) is obtained by substituting $s=j\omega$ in the expression (2.7);

$$\bar{I}(j\omega) = \sum_i \beta_i \bar{I}_i \bar{H}_i^\dagger \frac{\bar{V}(j\omega)}{j\omega - s_i} \tag{2.10}$$

where

$$\bar{V}(j\omega) = [V_m] \tag{2.11a}$$

$$E_0(s) = E_0 \tag{2.11b}$$

and

$$V_m = -E_0 \sin\theta \, e^{-j\frac{\omega}{c}\cos\theta \, z_m} \tag{2.11c}$$

The time domain solution is obtained by taking the Laplace inverse of the expression (2.7)

$$\bar{I}(t) = \frac{1}{2\pi j} \int_{C_B} \sum_i \beta_i \bar{I}_i \bar{H}_i^{\dagger} \frac{\bar{V}(s)e^{st}}{s-s_i} \, ds \tag{2.12}$$

where C_B is the Bromwich contour in the complex s-plane (Figure 2). Hence from equation (2.12)

$$\bar{I}(t) = \sum \beta_i \bar{I}_i \bar{H}_i^{\dagger} \bar{v}_i(t) \tag{2.13}$$

where

$$\bar{v}_i(t) = [v_{mi}(t)]$$

$$v_{mi}(t) = \frac{1}{2\pi j} \int_{C_B} \frac{V_m(s)e^{st}}{s-s_i} \, ds \tag{2.14}$$

For a step function plane wave incident, $E_0(s)$ in (2.5) is equal to E_0/s. Therefore, the expression (2.14) becomes

$$v_{mi}(t) = \frac{1}{2\pi j} \int_{C_B} \frac{M}{s(s-s_i)} e^{\frac{s}{c}[ct-\cos\theta \, z_m]} \, ds \tag{2.15}$$

where

$$M = -E_0 \sin\theta$$

Expanding (2.15) in terms of partial fractions yields

$$v_{mi}(t) = \frac{1}{2\pi j} \int_{C_B} M\, e^{\frac{s}{c}\left[ct-\cos\theta\, z_m\right]} \left[\frac{1}{s_i(s-s_i)} - \frac{1}{s_i s}\right] ds \qquad (2.16)$$

The contour integral (2.16) can be evaluated using the Cauchy residue theorem either by closing the Bromwich contour C_B along C_∞^+ or C_∞^- in Figure 2, depending on the sign of the exponent term $ct-\cos\theta\, z_m$. Because of the fact that all poles are located in the left half plane, for $ct<\cos\theta\, z_m$, the integral (2.16) is zero because the path may be taken along $C_B+C_\infty^+$ in the right half plane. For $ct>\cos\theta\, z_m$, closing the contour C_B along C_∞^- in the left half plane so that all the poles are included, (2.16) becomes

$$v_{mi}(t) = \frac{M}{s_i} u(\tau)\left[e^{\frac{s_i}{c}\tau} - 1\right] \qquad (2.17)$$

where

$$\tau = ct - \cos\theta\, z_m$$

Because of the appearance in (2.17) of the Heaviside unit step function $u(\tau)$, the expression exhibits a causality behavior. Substituting (2.17) into (2.13), the time domain solution is obtained.

2-3 Numerical results for finite circular cylinder in free space

The results of the application of SEM to the circular cylinder

are presented in this section for a cylinder of diameter to length ratio of 2a/L=0.01.

Figure 5 shows the location of the resonant frequencies of an isolated circular cylinder in free space. Basically, they appear in layers parallel to the jω-axis and the poles closest to the jω-axis are located at approximately

$$\frac{\omega L}{2c} \approx \frac{m\pi}{2} \quad , \quad m = 1, 2, 3, \cdots$$

as one might expect from the well-known fact that dipole antennas are resonant at frequencies such that the dipole is approximately an integer multiple of a half wavelength in length. In order to have a real response in the time domain, the poles must occur in complex conjugate pairs and in the figure only the upper left half s-plane poles are shown. There are, of course, no singularities in the right half of the s-plane. The resonant frequencies are dependent only on the shape of the structure, viz., the length and its radius. They should, of course, be relatively independent of the type of formulation and the numerical procedure used to determine them. Table 1 gives the results of the first few resonant frequencies closest to the jω-axis as determined by different types of integral equation formulations and current expansion sets:

a) Pocklington type integral equation, piecewise linear current expansion set, differential operator replaced by finite differences and point matching (Section 2.1)

b) Pocklington type integral equation, piecewise sinusoidal current expansion set with weighting functions chosen to be the same as the expansion set (Galerkin solution [4])

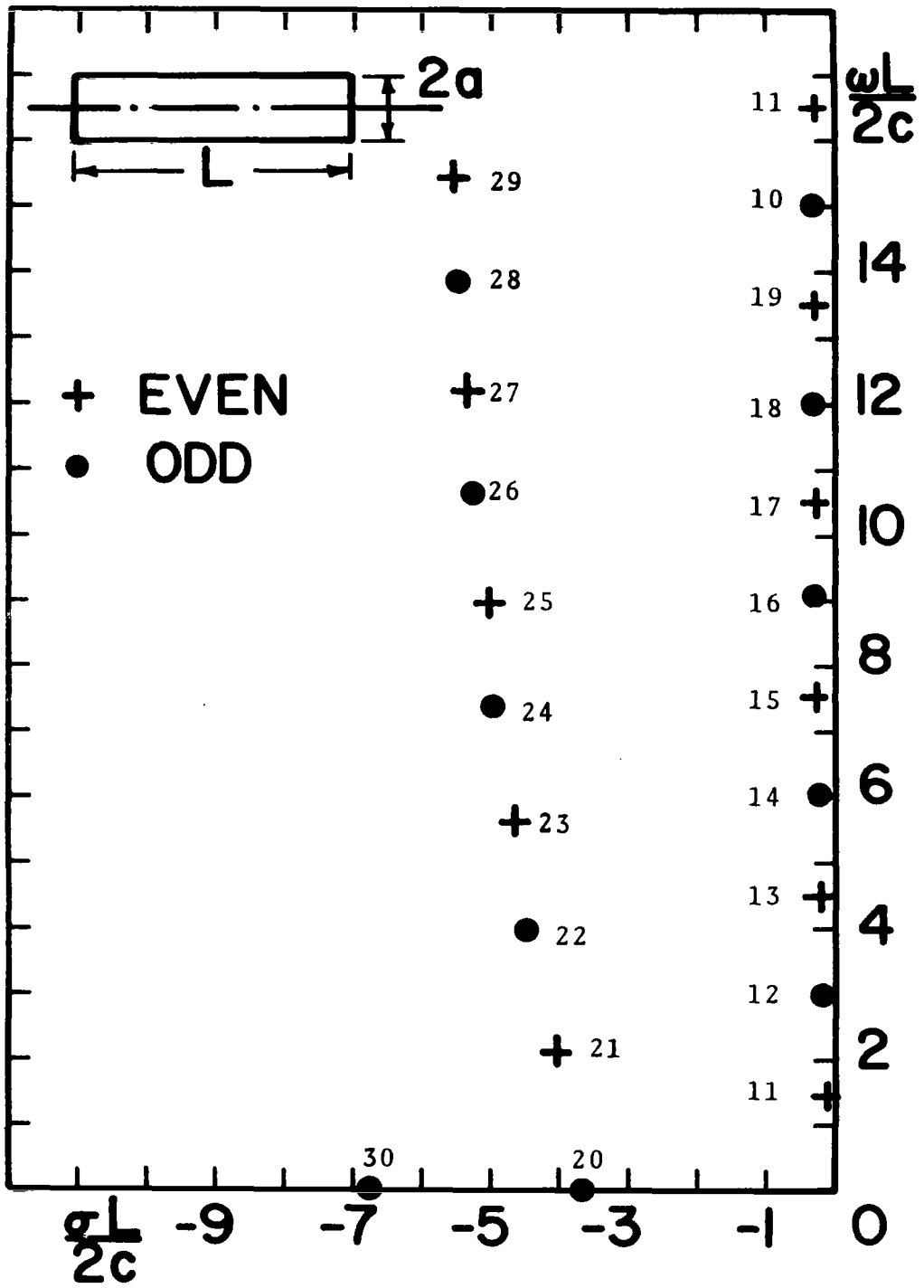

Figure 5. Natural frequencies of circular cylinder, a/h = 0.01.

CASES		(a)		(b)		(c)		(d)	
ℓ	n	$\frac{\sigma L}{2c}$	$\frac{\omega L}{23}$	$\frac{\sigma L}{2c}$	$\frac{\omega L}{2c}$	$\frac{\sigma L}{2c}$	$\frac{\omega L}{2c}$	$\frac{\sigma L}{2c}$	$\frac{\omega L}{2c}$
1	1	-0.1285	1.4363	-0.1283	1.4363	-0.1262	1.4355	-0.1201	1.4400
	2	-0.1887	2.9627	-0.1882	2.9630	-0.1870	2.9601	-0.1760	2.9909
	3	-0.2304	4.4946	-0.2300	4.4949	-0.2281	4.4896	-0.2202	4.5003

Table 1. Natural frequencies of circular cylinder, a/h = 0.01.

c) Hallén type integral equation, pulse current expansion set and point matching [5]

d) Hallén type integral equation, entire domain current expansion set (Tillman's sinusoidal basis set) and point matching [6]

Figures 6 and 7 show the trajectories of the first and the second resonant frequencies as the radius of the structure is increased. The poles move away from the $j\omega$-axis indicating that more damping is introduced as the structure becomes thicker. As the structure gets thicker, one should take into account the end effects. Figure 8 shows the location of the poles for a thicker case $2a/L=0.1$. These are obtained according to the method discussed in [7] using Pocklington type integral equation with piecewise sinusoidal basis set and point matching. Flat end caps are included at both ends of the structure and their effects are taken into account using quasi-static approximations.

It is also a matter of interest to analyze a prolate spheroid and compare its resonant frequencies in the limit as the eccentricity approaches unity with those of a thin wire structure. Figure 9 shows the pole locations for a thin prolate spheroid $2b/L=0.1407$ as determined from the Pocklington formulation [7], treating the structure as a body of revolution. In the limit as the reciprocal eccentricity e approaches unity, the pole locations of the prolate spheroid, indeed, approach the pole locations of the thin circular cylinder. The trajectories of a few of the axial resonances of a prolate spheroid as a function of the reciprocal eccentricity are

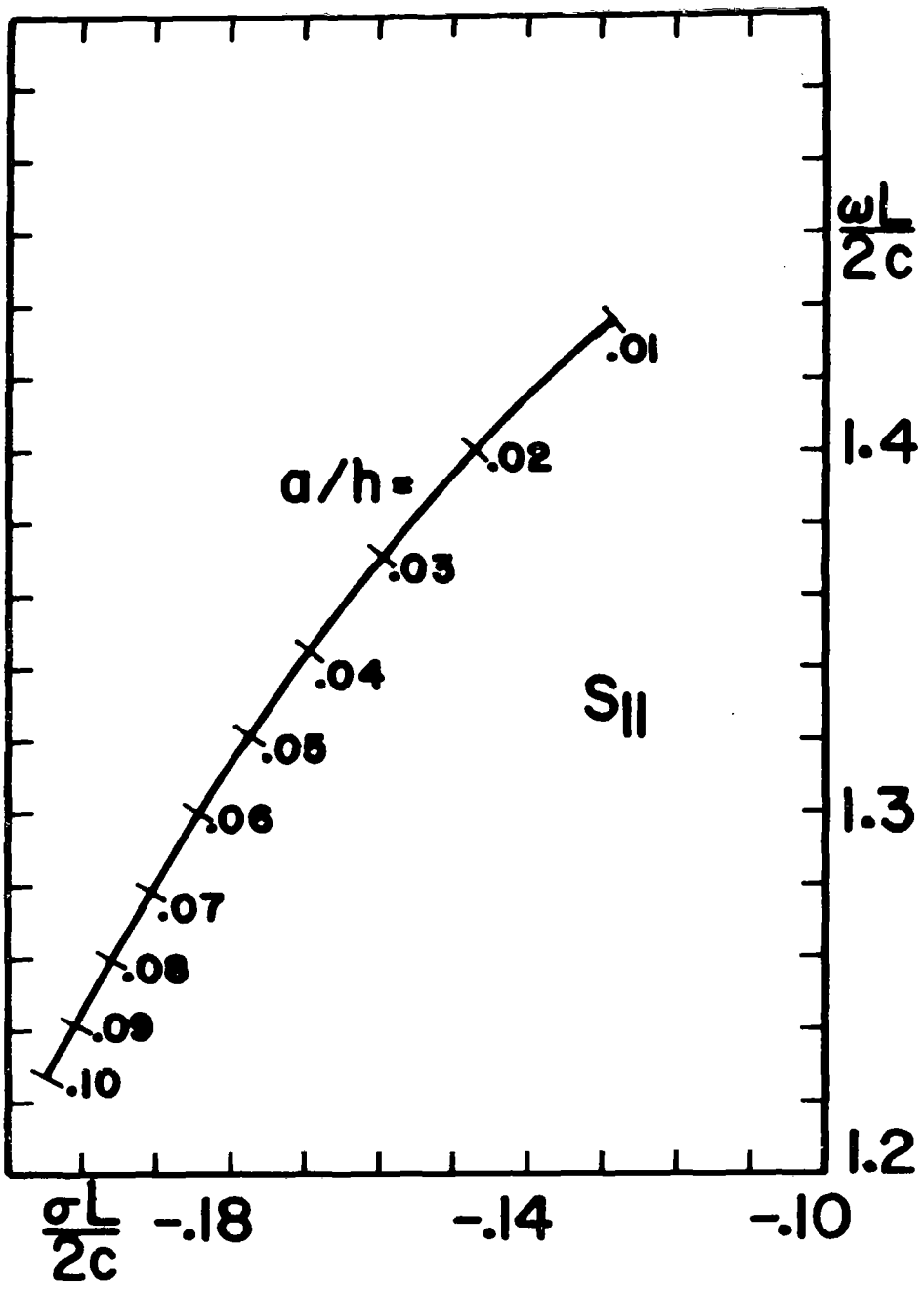

Figure 6. Trajectory of the pole s_{11} as a function of radius of the circular cylinder

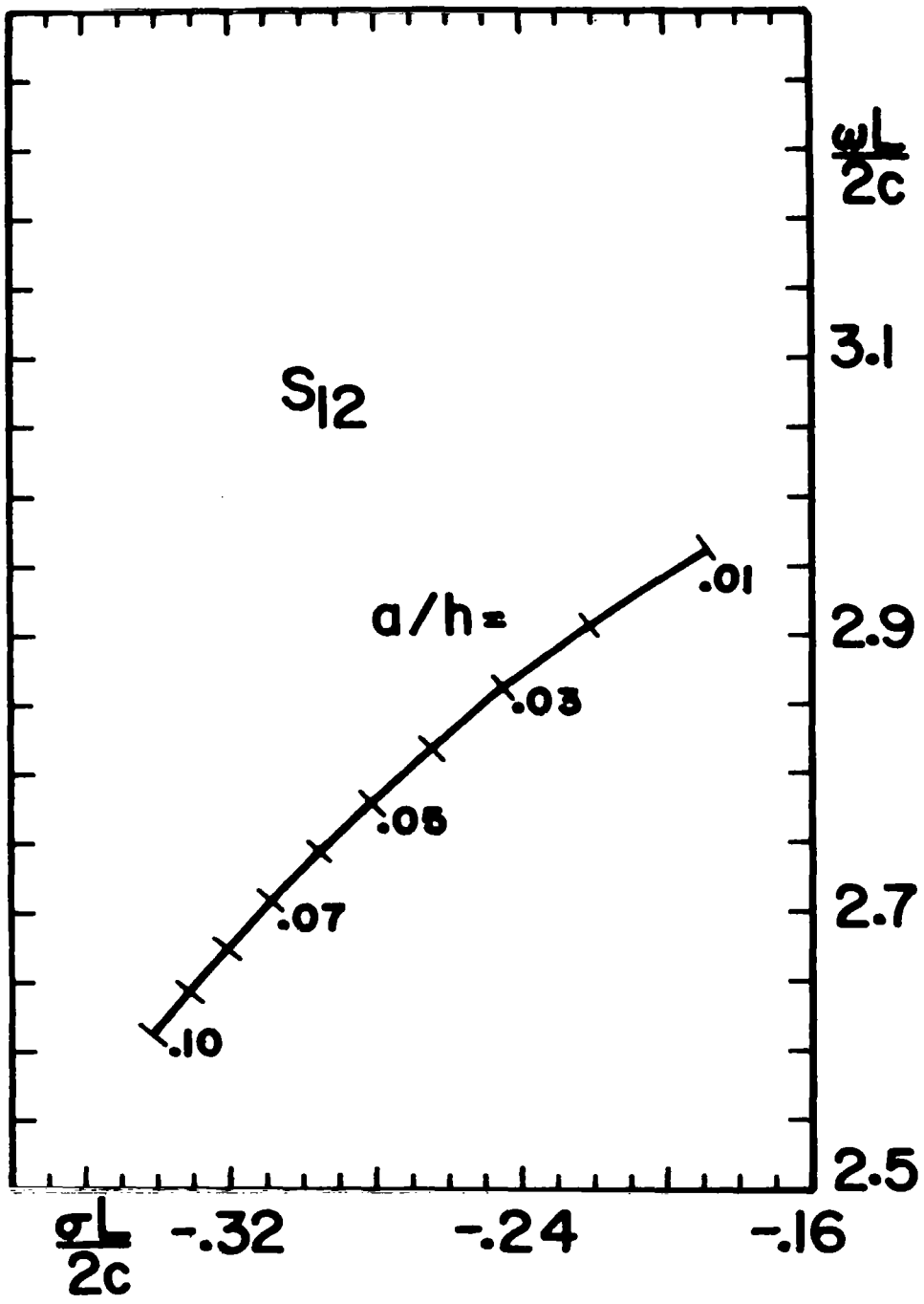

Figure 7. Trajectory of the pole s_{12} as a function of radius of the circular cylinder

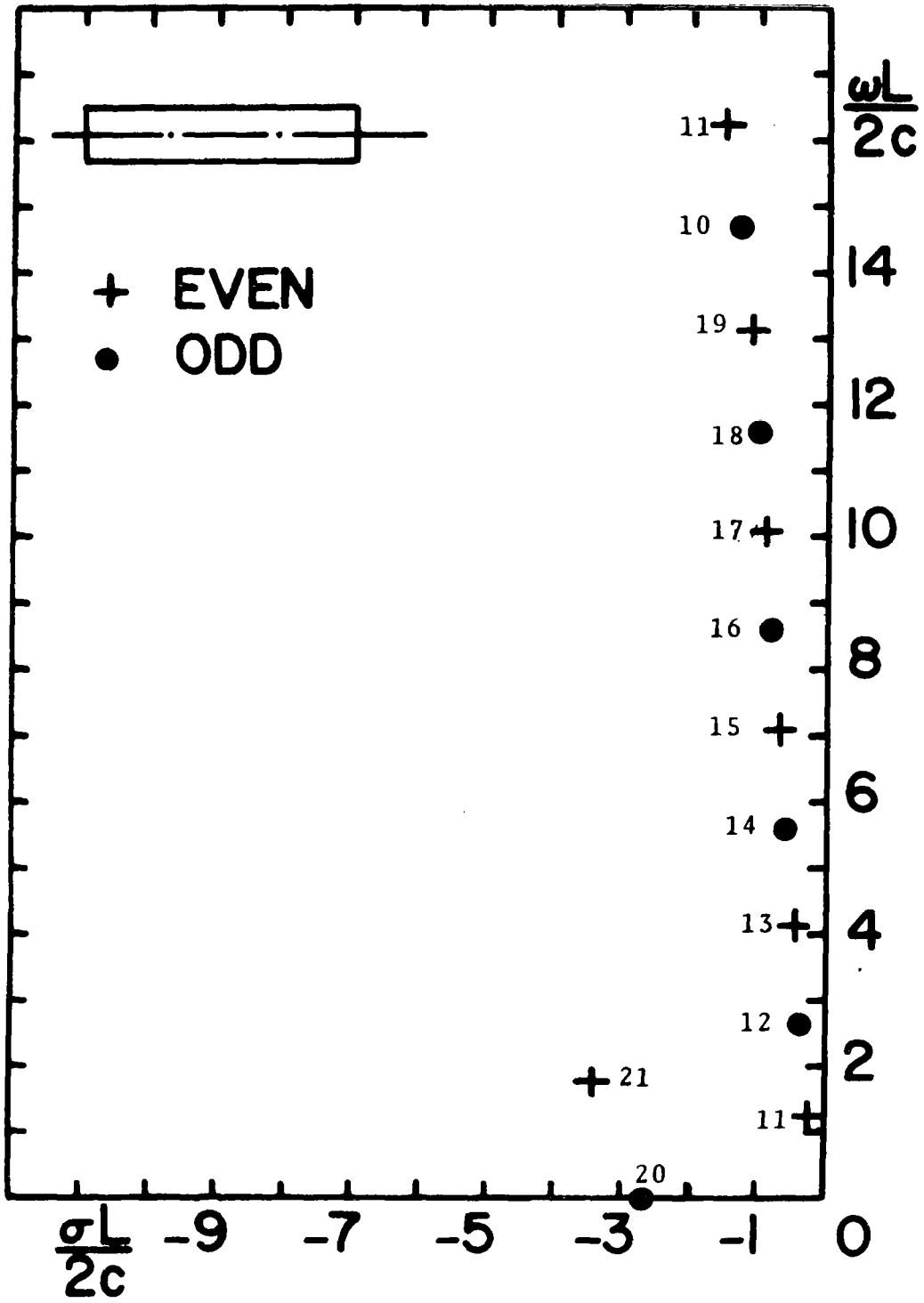

Figure 8. Natural frequencies of the circular cylinder, 2a/L = 0.1.

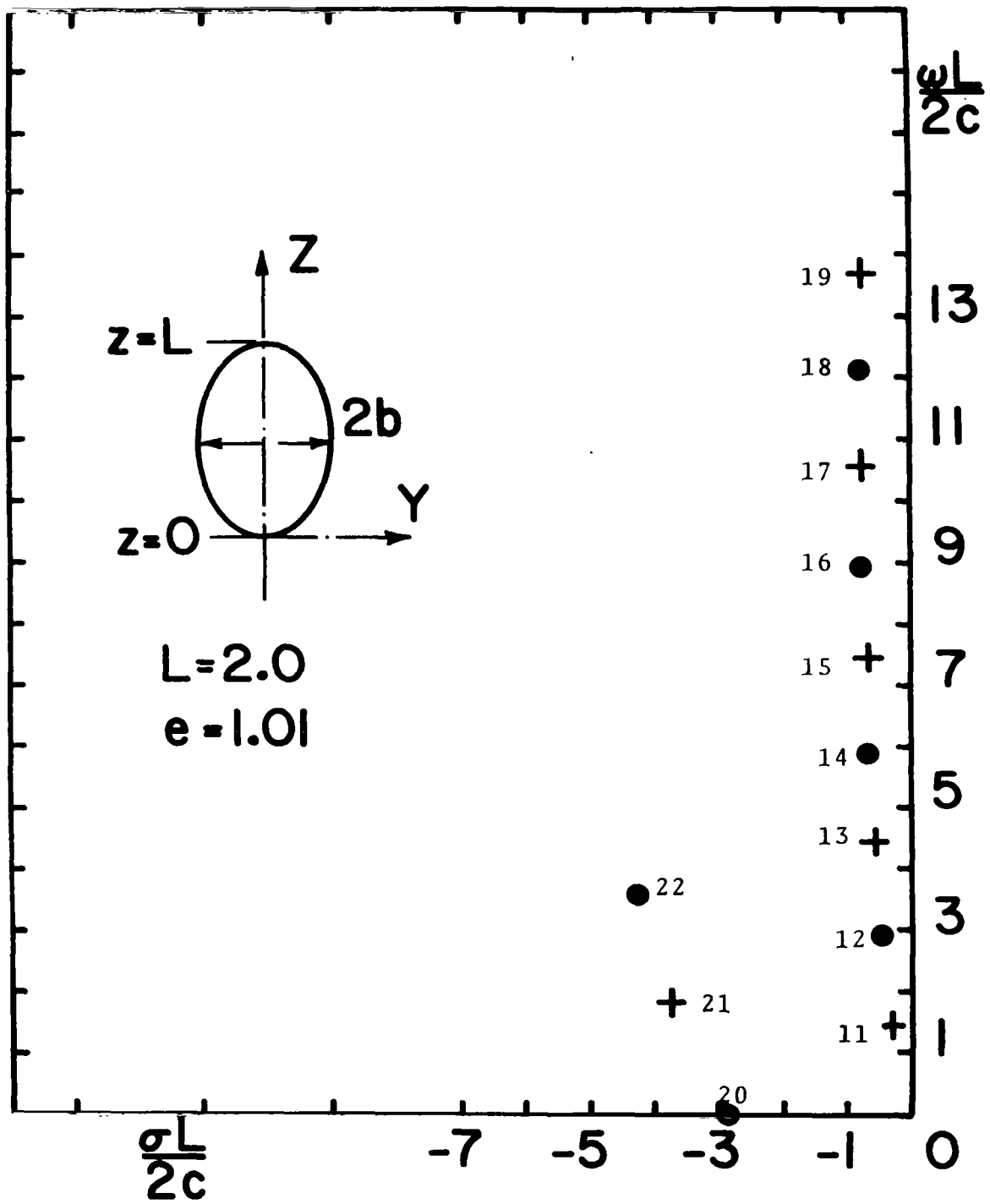

Figure 9. Natural frequencies of the prolate spheroid, 2b/L = 0.1407.

shown in Figure 10. As the center radius is increased, the object approaches a sphere in shape.

The real and imaginary parts of the first few natural modal current distributions corresponding to the poles of the circular cylinder closest to the $j\omega$-axis are shown in Figure 11. For very thin structures, the real part dominates and is approximately sinusoidal.

In Figure 12 and 13, the frequency domain solution obtained from SEM calculations at different points on the structure is given corresponding to a time harmonic plane wave incident and the results are compared at the center of structure by solving the integral equation by direct moment method solution. Also in Figures 14 and 15 are given the time domain current distribution as obtained by SEM for E_θ-polarization with a step function plane wave incident and these results are checked at the center point by direct Fourier inversion of the frequency domain data obtained by solving the integral equation.

Figure 16 shows the convergence of the time domain current at $z/L=0.75$ as the number of poles closest to the axis is increased. As can be seen in the figure, the late time response corresponding to the time $ct/L>3$, can be constructed with the 3 or 4 poles closest to the $j\omega$-axis.

2-4 Finite circular cylinder parallel to conducting ground plane

In this section a finite circular conducting cylinder placed parallel to a perfectly conducting ground plane is analyzed by SEM

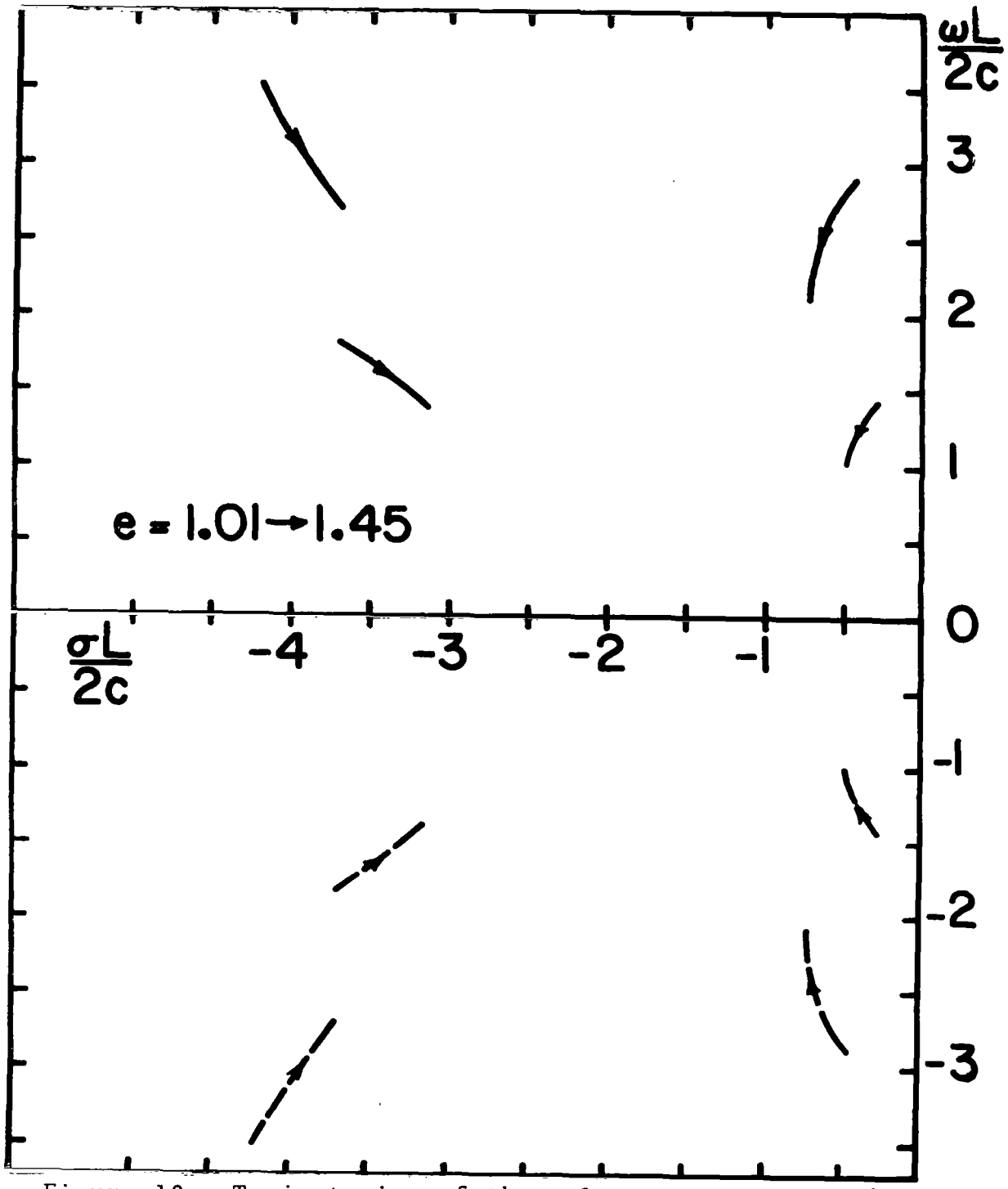

Figure 10. Trajectories of the poles s_{11}, s_{12}, s_{21} and s_{22} as a function of reciprocal eccentricity of the prolate spheroid.

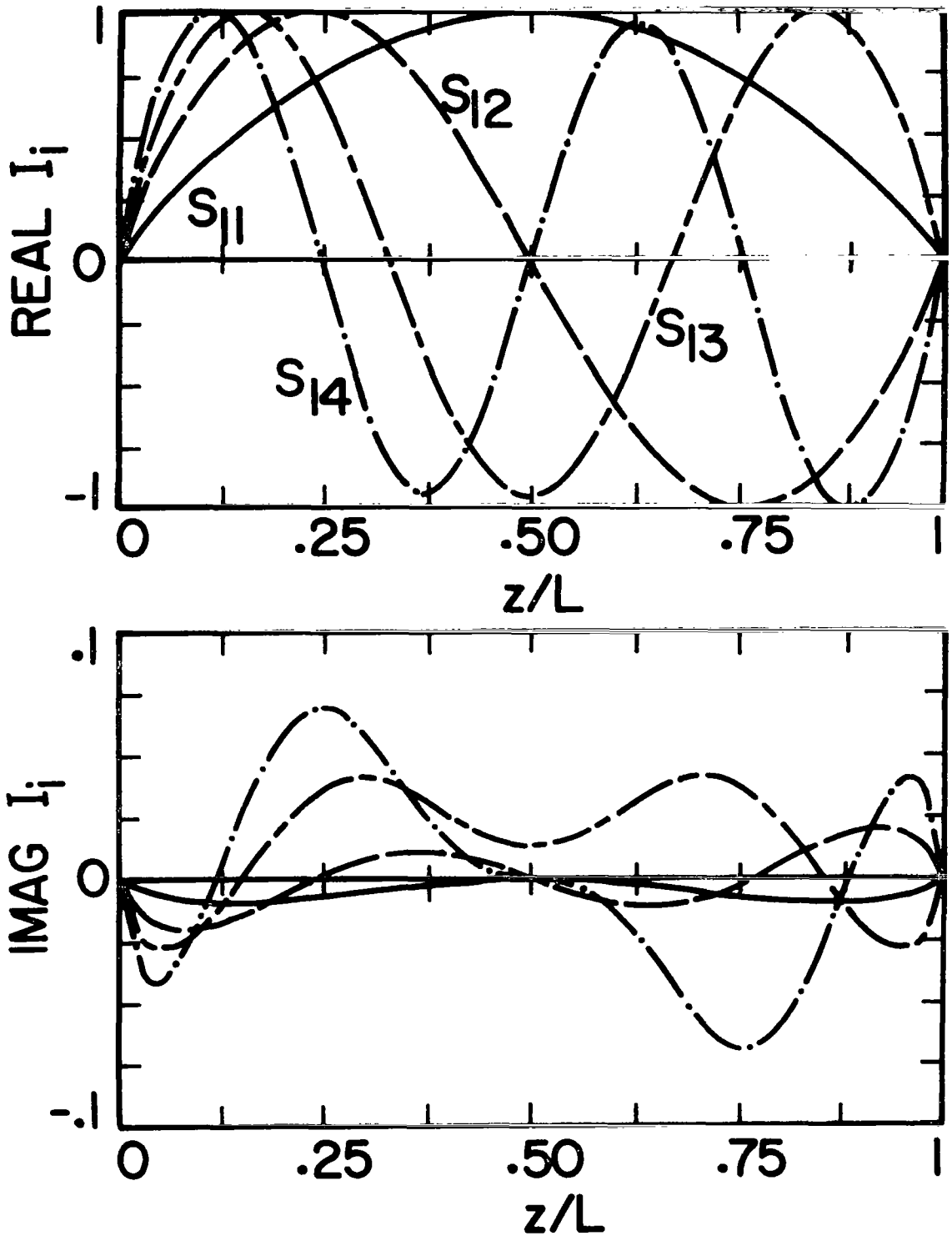

Figure 11. Current distribution of natural modes of circular cylinder for resonant frequencies s_{11}, s_{12}, s_{13}, and s_{14}, 2a/L = 0.01.

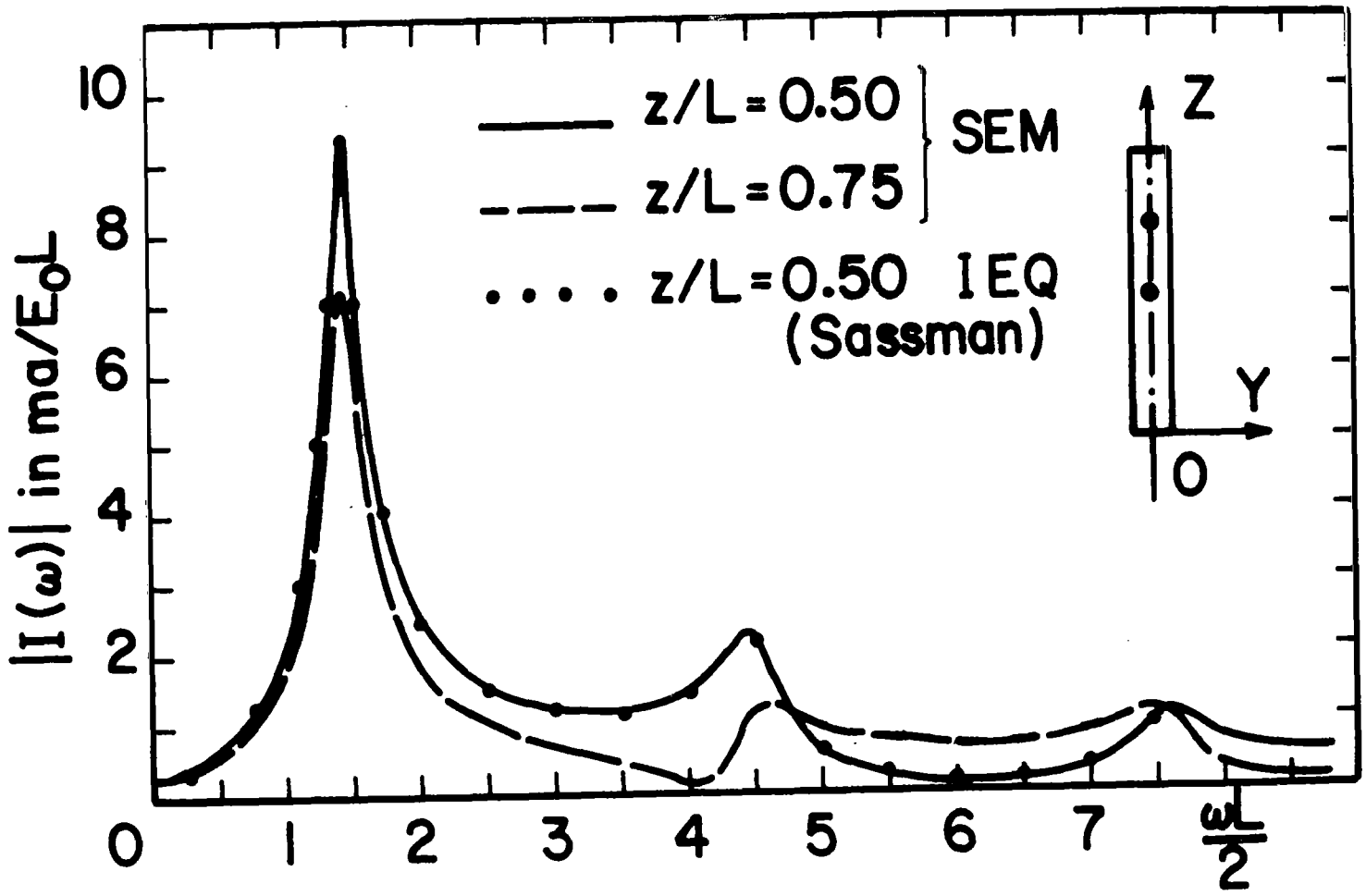

Figure 12. Variation of current on the circular cylinder as a function of frequency for a plane wave incident, $\theta = 90°$, $2a/L = 0.01$.

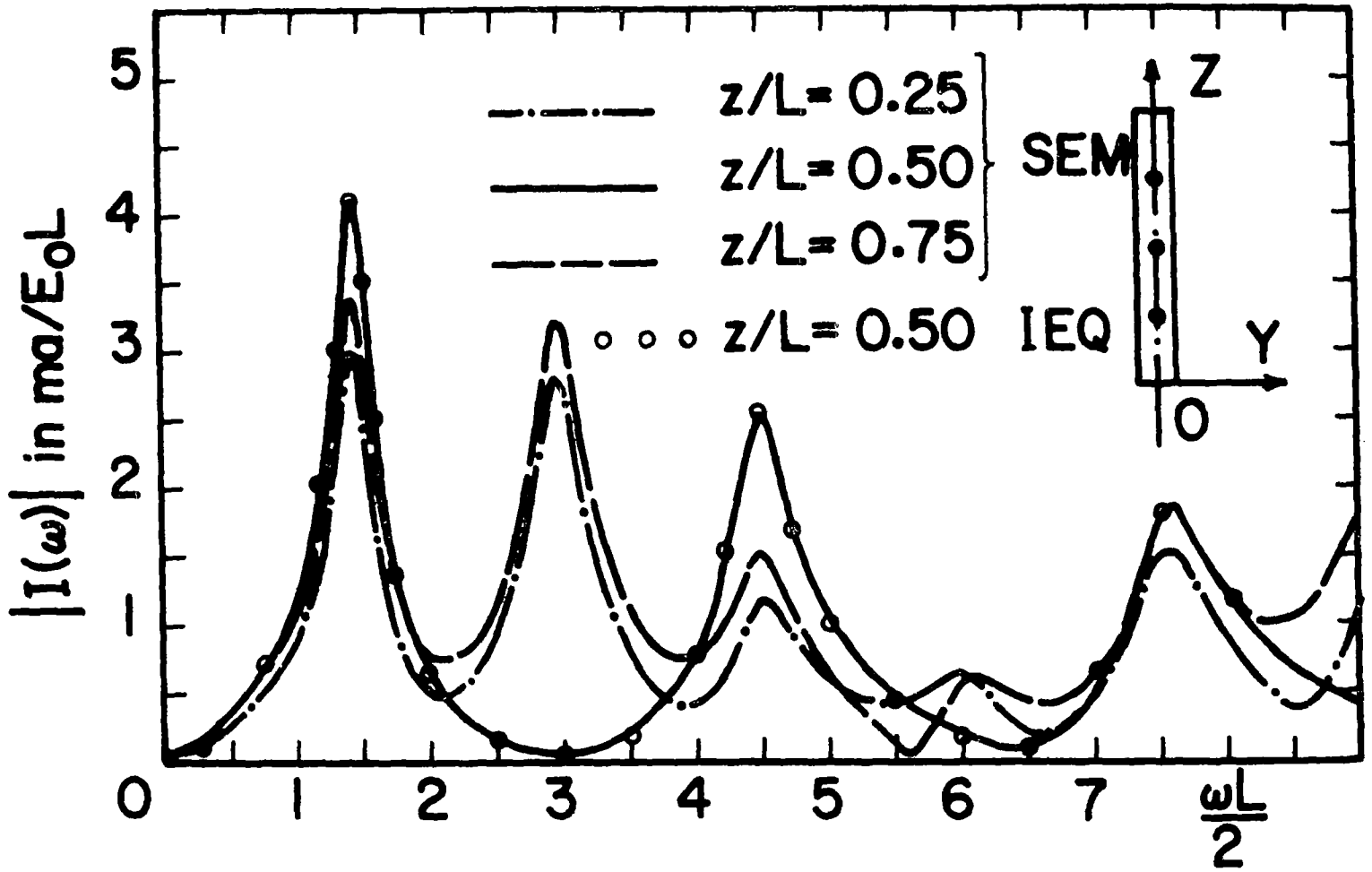

Figure 13. Variation of current on the circular cylinder as a function of frequency for a plane wave incident, $\theta = 30°$, $2a/L = 0.01$.

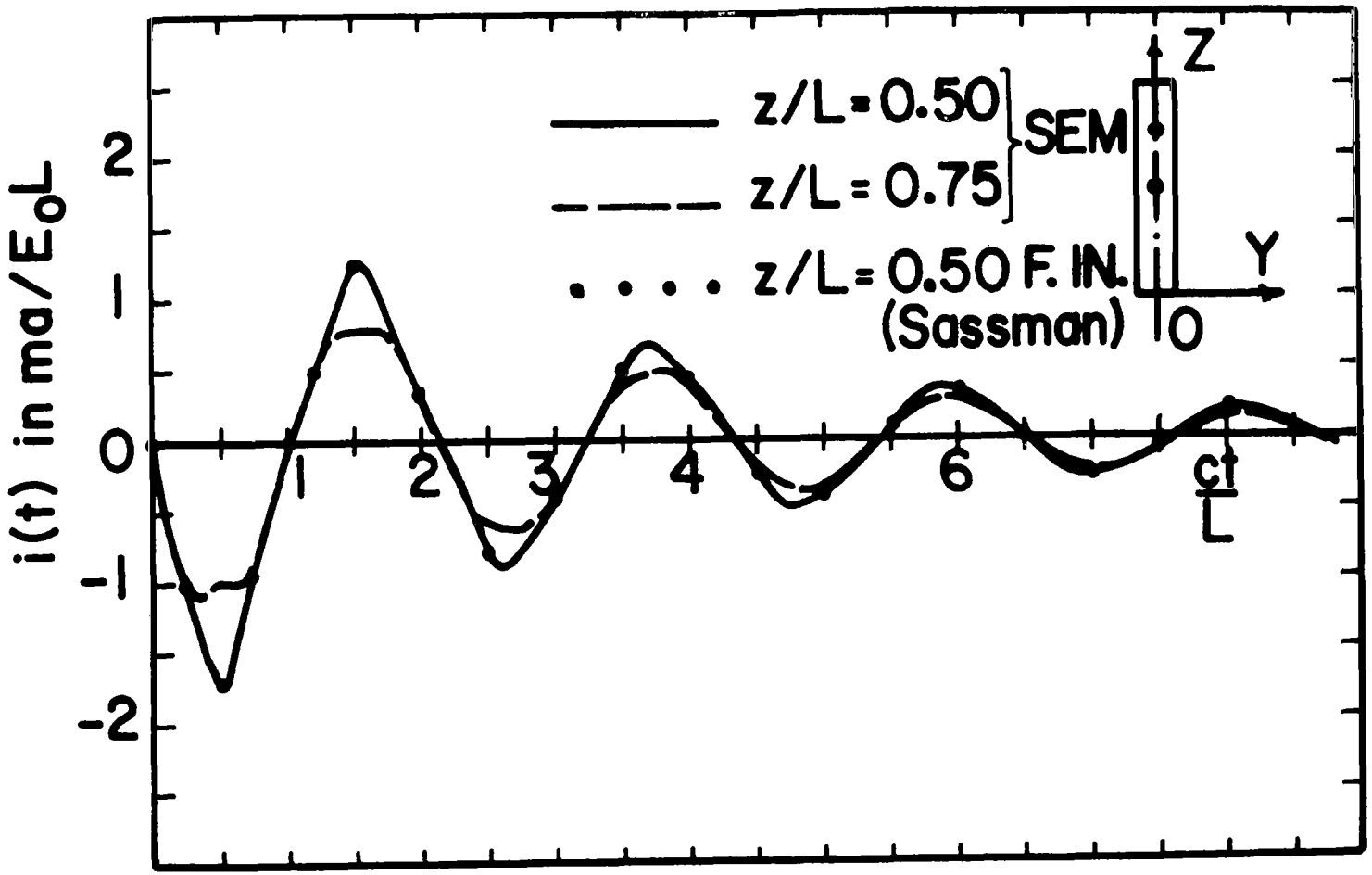

Figure 14. Time domain current, step function plane wave incident, $\theta = 90°$, $2a/L = 0.01$.

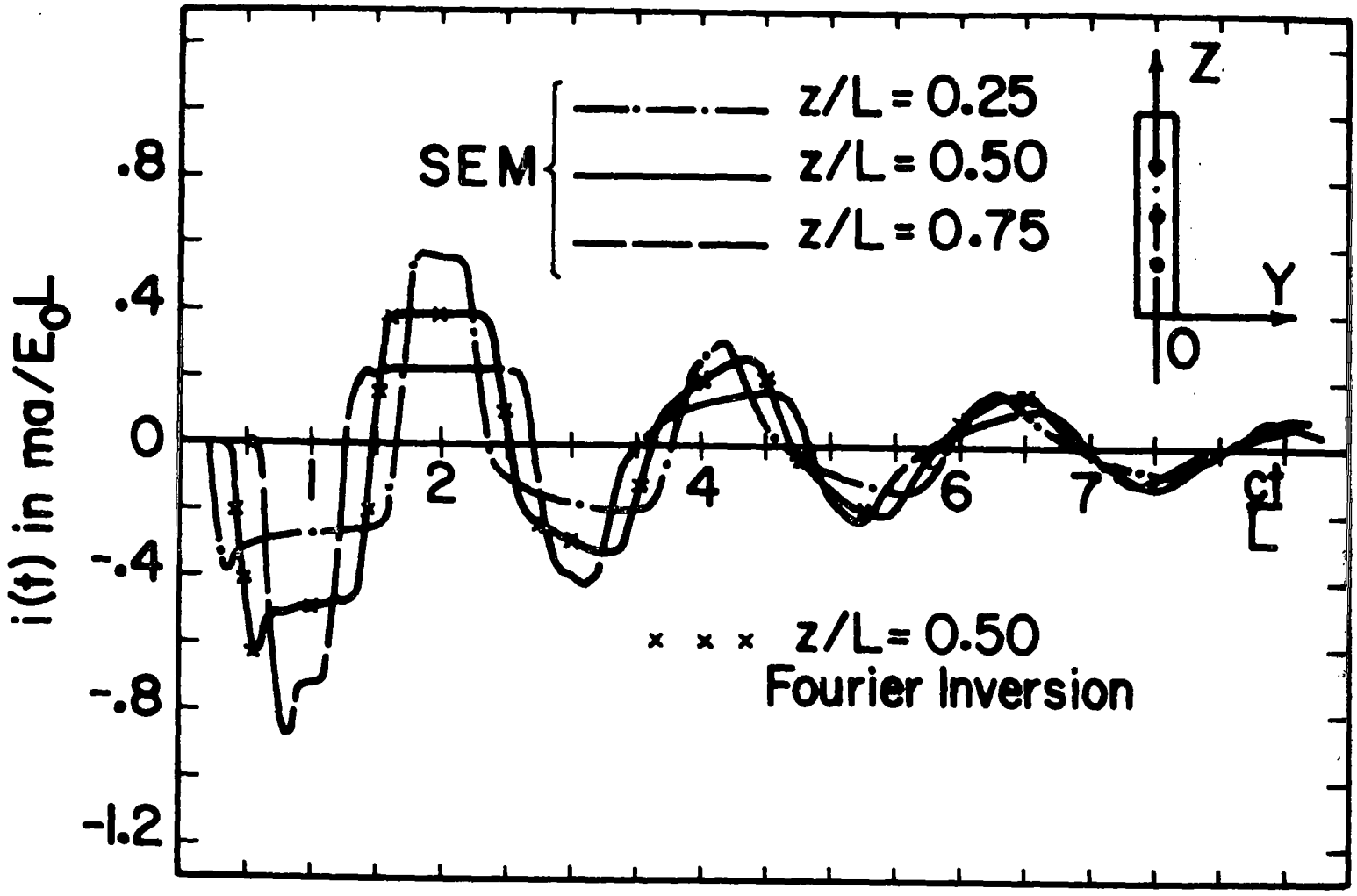

Figure 15. Time domain current, step function plane wave incident, $\theta = 30°$, $t = 0$ at $z = 0$.

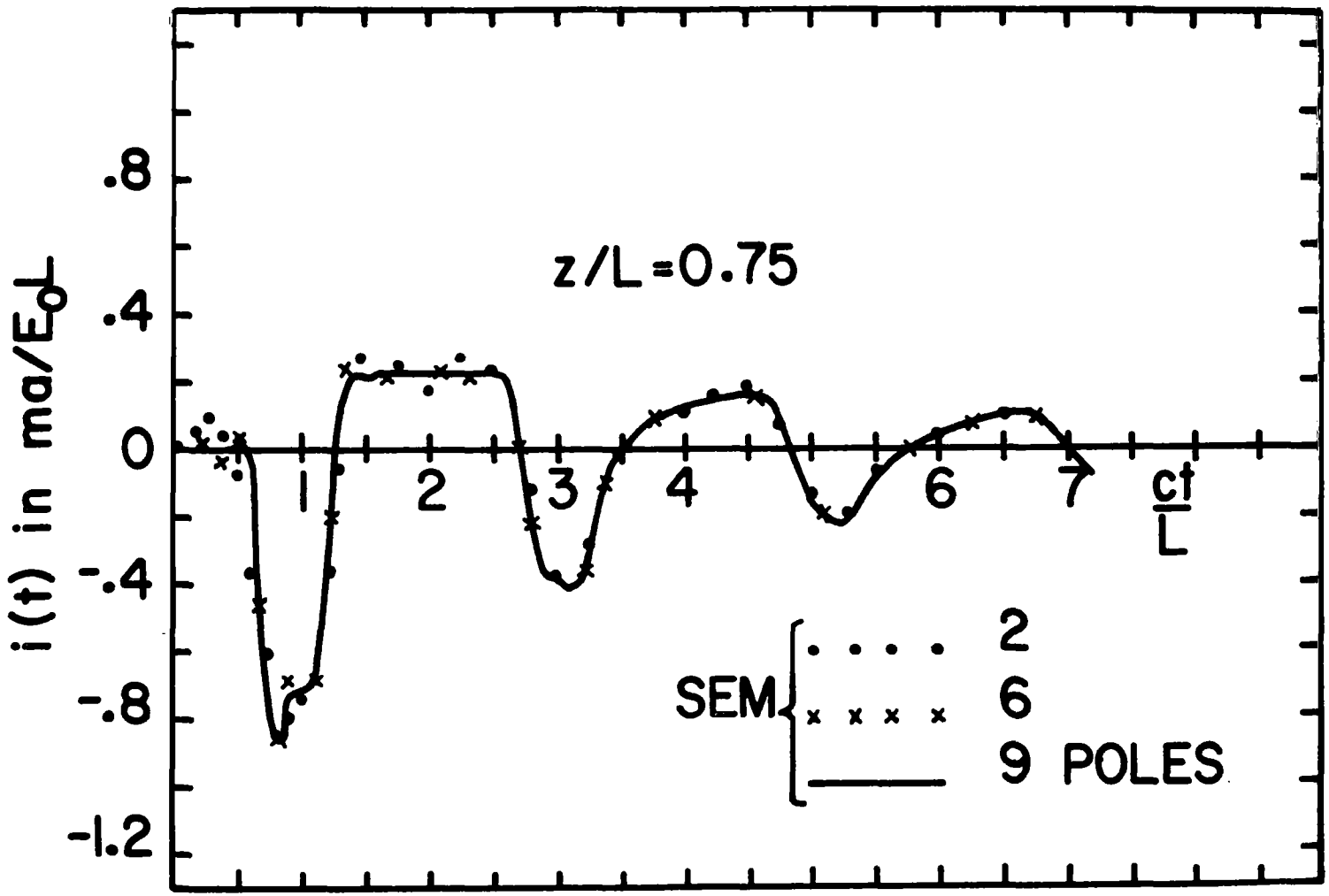

Figure 16. Convergence of time domain current, $\theta = 30°$, E_θ-polarization, step function plane wave incident, $t = 0$ at $z = 0$, $2a/L = 0.01$.

and the results are presented showing the effect of the ground plane on the resonant frequencies and other transient scattering characteristics of the structure.

In Figure 17, a circular cylinder of total length L and of radius a is oriented along z axis. A perfectly conducting ground plane is placed parallel to the structure in the xz plane at a distance y=d. A Pocklington type integro-differential equation for the currents induced can be developed for the circular cylinder over the ground plane similar to that developed for the isolated case (equation 2.1) with appropriate modifications to take into account the effect of the ground plane. Applying image theory, the ground plane is removed and an image structure is placed at y=2d. If $I_z(z,s)$ is the induced current distribution on the structure corresponding to the incident z component of the electric field, $E_z^i(z,s)$, equal and opposite currents are induced on the image structure, so that only the kernel function in the integral equation (2.1) is modified. Hence the Pocklington E-field type integral equation for the circular cylinder placed parallel to a perfectly conducting ground plane is obtained as

$$-4\pi s\epsilon_0 E_z^i(z,s) = \left[\frac{\partial^2}{\partial z^2} - \gamma^2\right] A^g(z,s) \qquad (2.19)$$

and

$$A^g(z,s) = \int_0^L I_z(z',s) K^g(z,z's)\, dz'$$

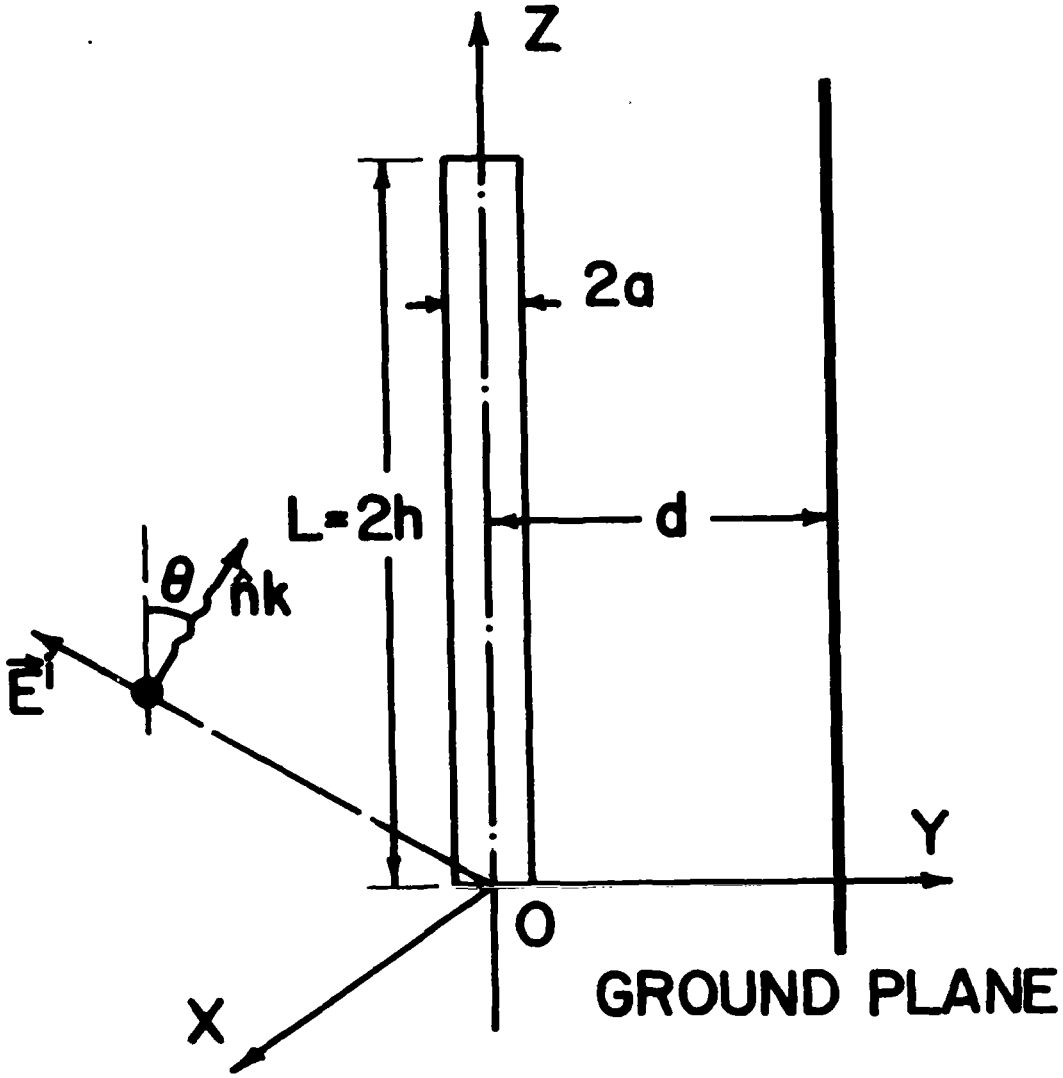

Figure 17. Geometry of circular cylinder parallel to a conducting ground plane.

where $K^g(z,z's)$ is the kernel function defined as

$$K^g(z,z's) = \frac{e^{-\gamma R}}{R} - \frac{e^{-\gamma R^1}}{R^1} \tag{2.20}$$

and

$$R^2 = a^2 + (z-z')^2 \tag{2.21a}$$

$$R^{1^2} = a^2 + 4d^2 + (z-z')^2 \tag{2.21b}$$

$$\gamma = \frac{s}{c} \tag{2.21c}$$

For E_θ-polarization, the incident electric field along the z direction is given by equation (2.5) plus the reflected field term due to the ground plane, viz.,

$$E_z^i(z,s) = -E_0(s) \sin\theta \, e^{-\gamma \cos\theta \, z} \cdot \left[1 - e^{-\gamma \sin\theta \, (2d)}\right] \tag{2.22}$$

Paralleling the procedure followed for the isolated case, the integro-differential equation (2.19) can be solved by the method of moments for the currents induced on the cylinder over the ground plane. In section 2.5 the results of SEM are presented. The frequency domain solution is again calculated by the expression (2.10) with the incident electric field term replaced with equation (2.22). Also the time domain solution for the circular cylinder over the ground plane is calculated using the expressions (2.13), (2.14) and (2.22)

$$\bar{I}(t) = \sum_i \beta_i \bar{T}_i \bar{H}_i^{\dagger} \bar{v}_i(t) \tag{2.23}$$

where

$$\bar{v}_i(t) = [v_{mi}(t)]$$

and

$$v_{mi}(t) = \frac{M}{s_i} u(\tau_1)\left[e^{\frac{s_i}{c}\tau_1} - 1\right] - \frac{M}{s_i} u(\tau_2)\left[e^{\frac{s_i}{c}\tau_2} - 1\right] \tag{2.24}$$

$$\tau_1 = ct - \cos\theta\, z_m \tag{2.25a}$$

$$\tau_2 = ct - \cos\theta\, z_m - 2d \sin\theta \tag{2.25b}$$

2-5 Numerical results for circular cylinder parallel to ground plane

In this section are presented the results of the application of SEM to a circular cylinder parallel to a conducting ground plane. Pole trajectories are given showing the influence of changing the distance above the ground plane. Also shown are modal currents and time domain and frequency domain current responses. It is found that the pole trajectories are considerably more complicated than in the case of an isolated cylinder.

Figure 18 gives the location of the complex natural frequencies and also serves to identify the indexing of the poles ($s_{\ell n}$ denotes the nth pole in the layer ℓ). Only the upper left half s-plane poles are shown in the figure and their complex conjugate counterparts

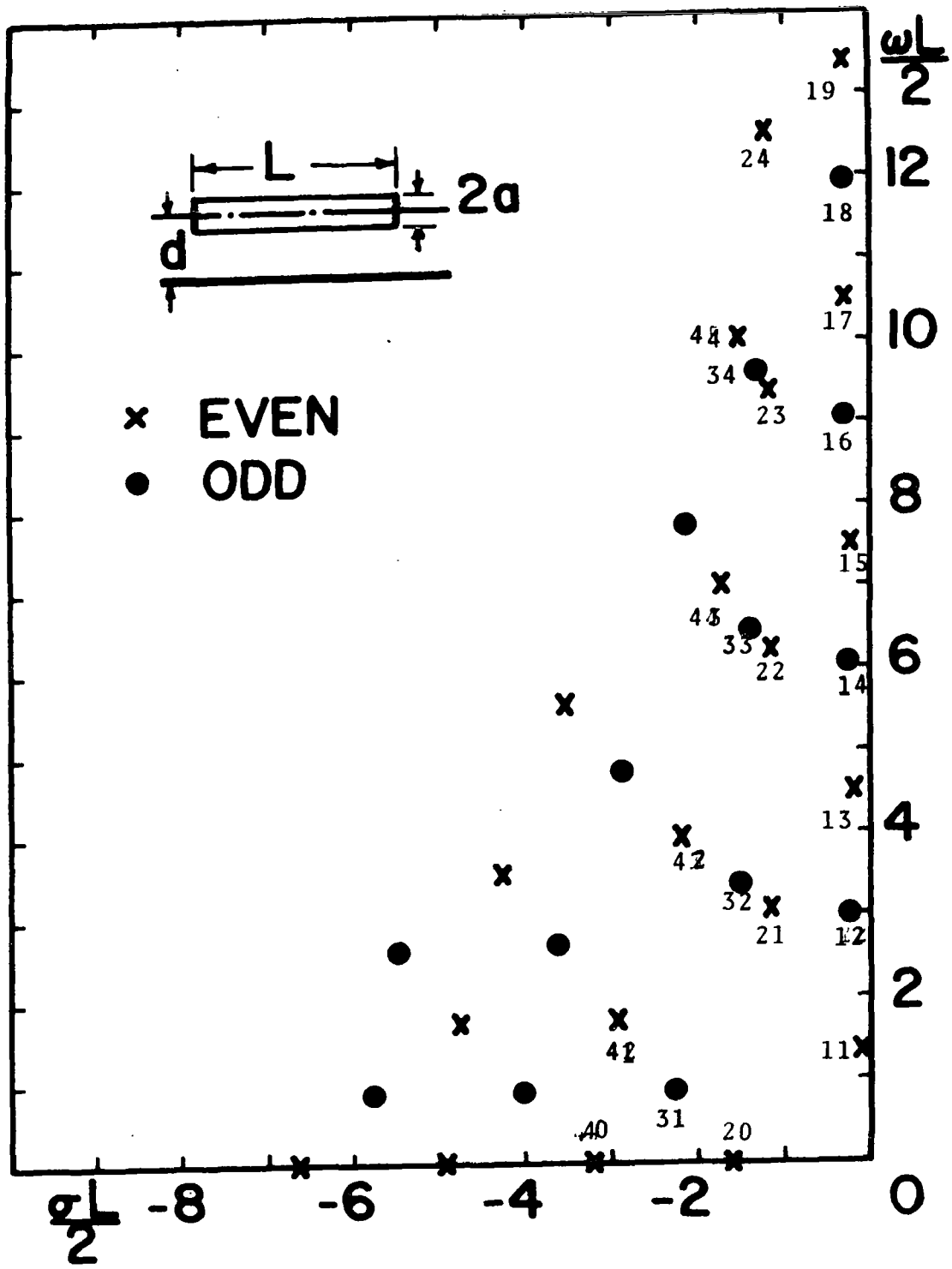

Figure 18. Natural frequencies of circular cylinder over ground plane, 2a/L = 0.01, 2d/L = 1.0.

are omitted. The poles appear to be located in layers parallel to the jω-axis, and those poles closest to the jω-axis (first layer) are slightly perturbed compared to those of the isolated case (Figure 5) but are still located roughly at

$$\frac{\omega L}{2c} \simeq \frac{m\pi}{2} \quad , \quad m = 1, 2, 3, \cdots,$$

The poles located in the remaining layers (ℓ=2,3, ...) are apparently due to the parallel interaction between the circular cylinder and its image. Furthermore, each pole is designated as either even or odd depending on the evenness or the oddness of the corresponding modal current distribution with respect to the center of the structure.

The trajectory of the pole s_{11} with the radius of the circular cylinder held constant and the distance d over the ground plane varied is shown in Figure 19. For the cylinder very close to the ground plane, the pole tends toward $\omega L/2c = \pi/2$, the first resonant frequency of the two wire transmission line formed by the wire and its image. As the distance above the ground increases, the trajectory appears to spiral around the pole location of the isolated case until another pole from the next layer passes sufficiently close to the spiral, in which case the two poles seem to exchange roles. That is, the original pole near the free space pole leaves the spiral path and begins to approach the origin while the new pole takes up the spiral trajectory left by the original pole. This pole makes only

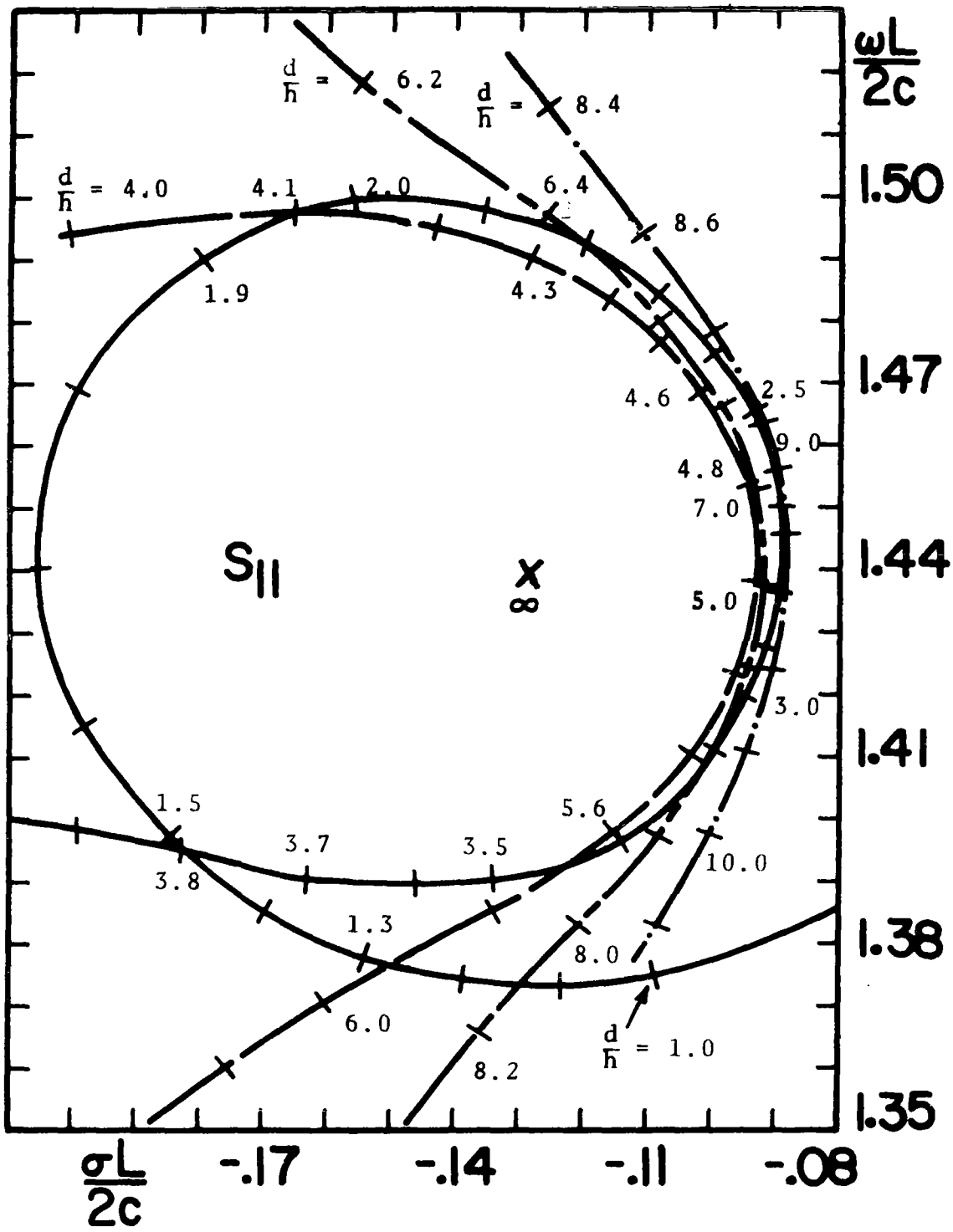

Figure 19. Trajectory of the pole s_{11} of circular cylinder as a function of distance over ground plane, 2a/L = 0.01.

one circuit around the free-space pole and then is in turn displaced by the next pole in the same layer. Thus, for any distance of the structure above the ground plane, there is only one pole circling the free space pole. From numerical studies, it was observed that the above trajectories further depend on the radius to length ratio of the structure. For comparatively thin structures, the s_{11} pole spirals many times around the pole location of the isolated case before another pole from next layer comes close enough to displace it. In Figure 20, the second and the third layer pole trajectories are traced. Observe that as the distance to the ground plane is increased, they tend to move towards s = 0. For thin structures, the second and third layer poles pass close to and interact with the s_{11} trajectory, but they ultimately miss the spiral path of s_{11} as distance d over the ground plane is increased. It was observed that the closer these secondary layer trajectories come to the region of the free-space pole the more perturbed the spirals become. The same trajectories are shown again in Figure 21, plotted with an alternative normalization. The normalization to distance above the ground plane in Figure 21 emphasizes the association of these poles with the interaction of the circular cylinder with its image, as seen by the relative insensitivity of the imaginary part of the normalized resonant frequency to changes in distance over the ground plane. We further note that the spacing between the pole trajectories is approximately $n\pi$ along the $\omega d/c$ axis, which is consistent with the

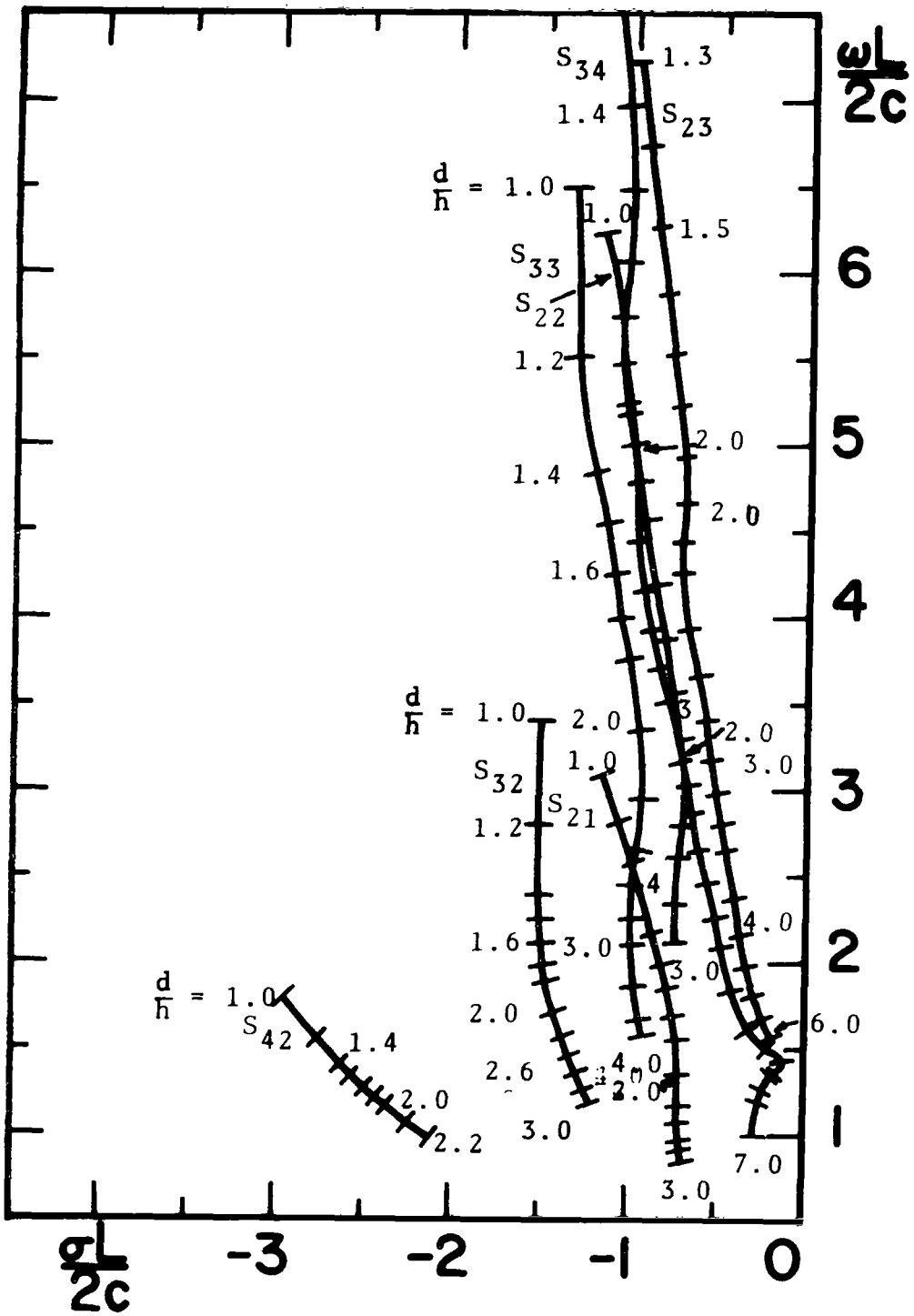

Figure 20. Trajectories of the second and third layer poles as a function of distance of circular cylinder from the ground plane, 2a/L = 0.01.

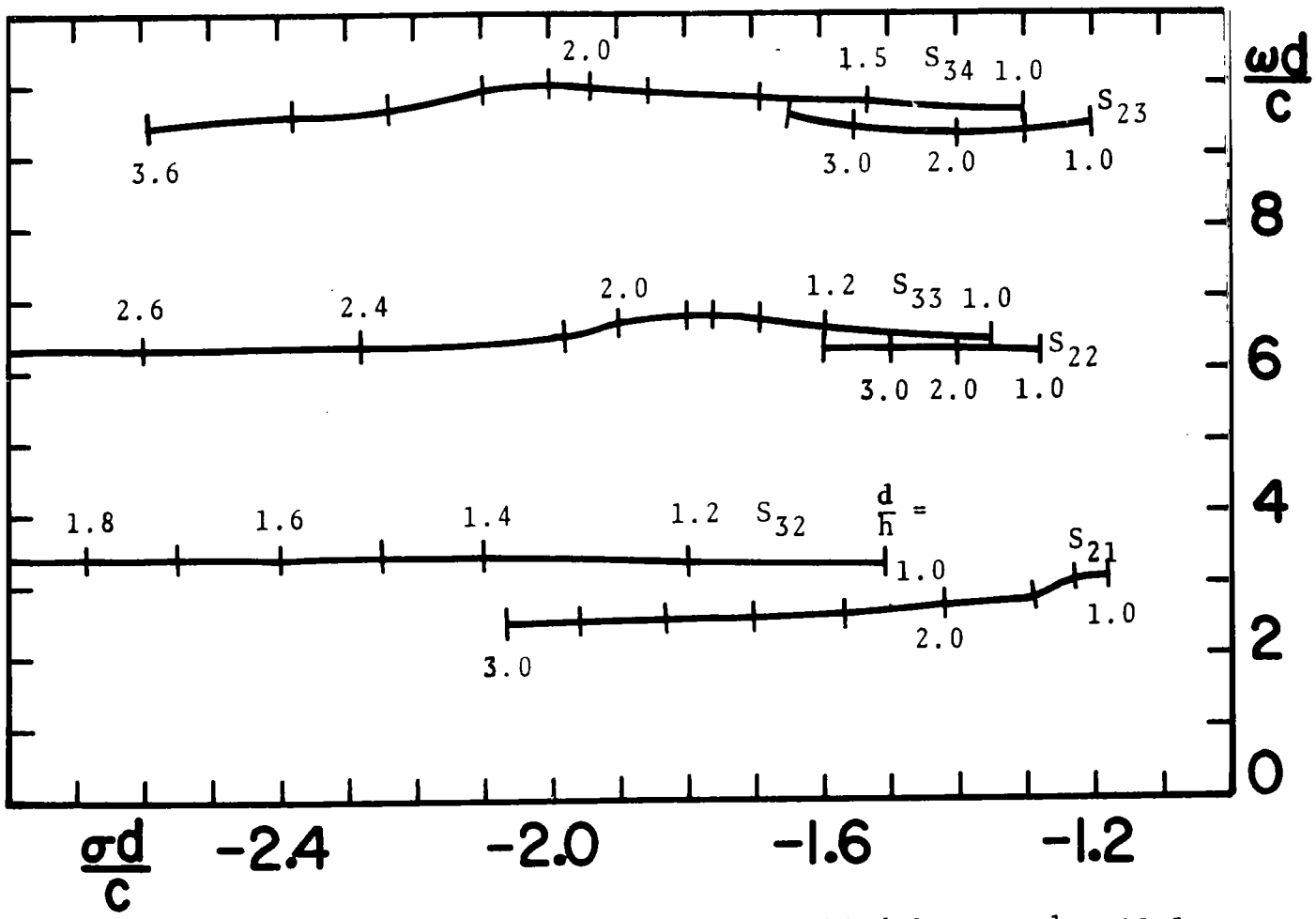

Figure 21. Trajectories of the second and third layer poles as a function of distance of circular cylinder over ground plane, plotted with distance d as scale factor, 2a/L = 0.01.

requirement that the cylinder-to-ground interaction should be approximately resonant when the spacing d is about a half wavelength or an integer multiple thereof. Further we note that the longer the wire, for a fixed distance d, the larger "Q" of the resonance, or equivalently, the smaller the damping constant. The s_{12} pole trajectory is shown in Figure 22 as the distance over the ground plane is increased. It spirals approximately at twice the rate of the s_{11} pole trajectory. If the structure is made slightly thicker, the s_{12} trajectory would behave similar to the s_{11} trajectory.

In Figure 23 are shown the real and imaginary parts of the modal current distributions corresponding to the first layer poles. The real part of the modal current distribution resembles closely that obtained for an isolated case (Figure 11). The modal current distribution along the circular cylinder is, of course, influenced by its distance over the ground plane, but the numerical results show that these influences are relatively minor. The magnitude of the modal current distribution of the second, third and fourth layer poles is shown in Figure 24. It is interesting to note that the modal current distribution of the second layer is similar to the modal current distribution of the first pole in the first layer (s_{11}) and this layer is the one whose poles interact with it. Similarly, the modal current distribution of the third and fourth layer poles resemble some-

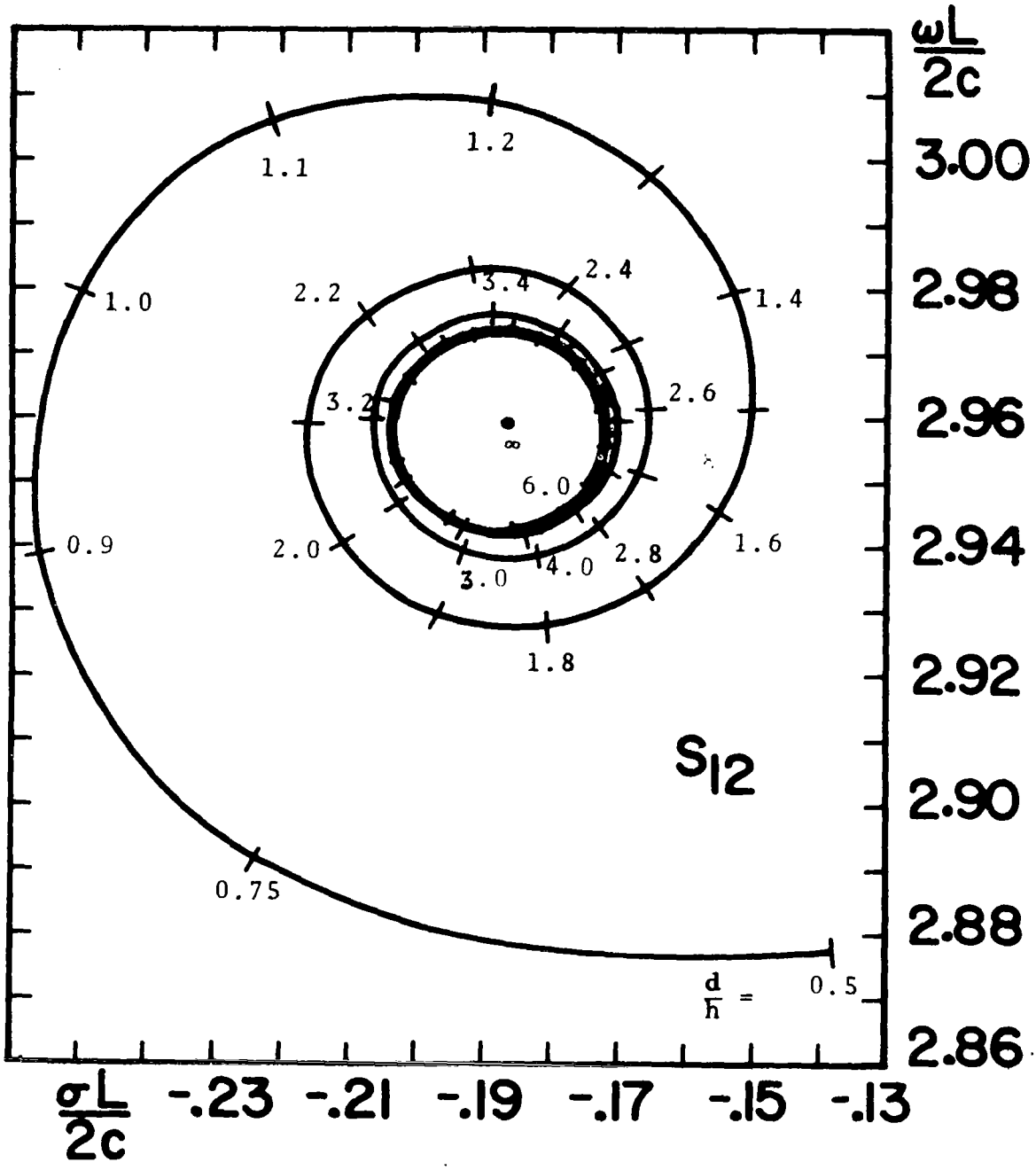

Figure 22. Trajectory of the pole s_{12} of circular cylinder as a function of distance over ground plane, 2a/L = 0.01.

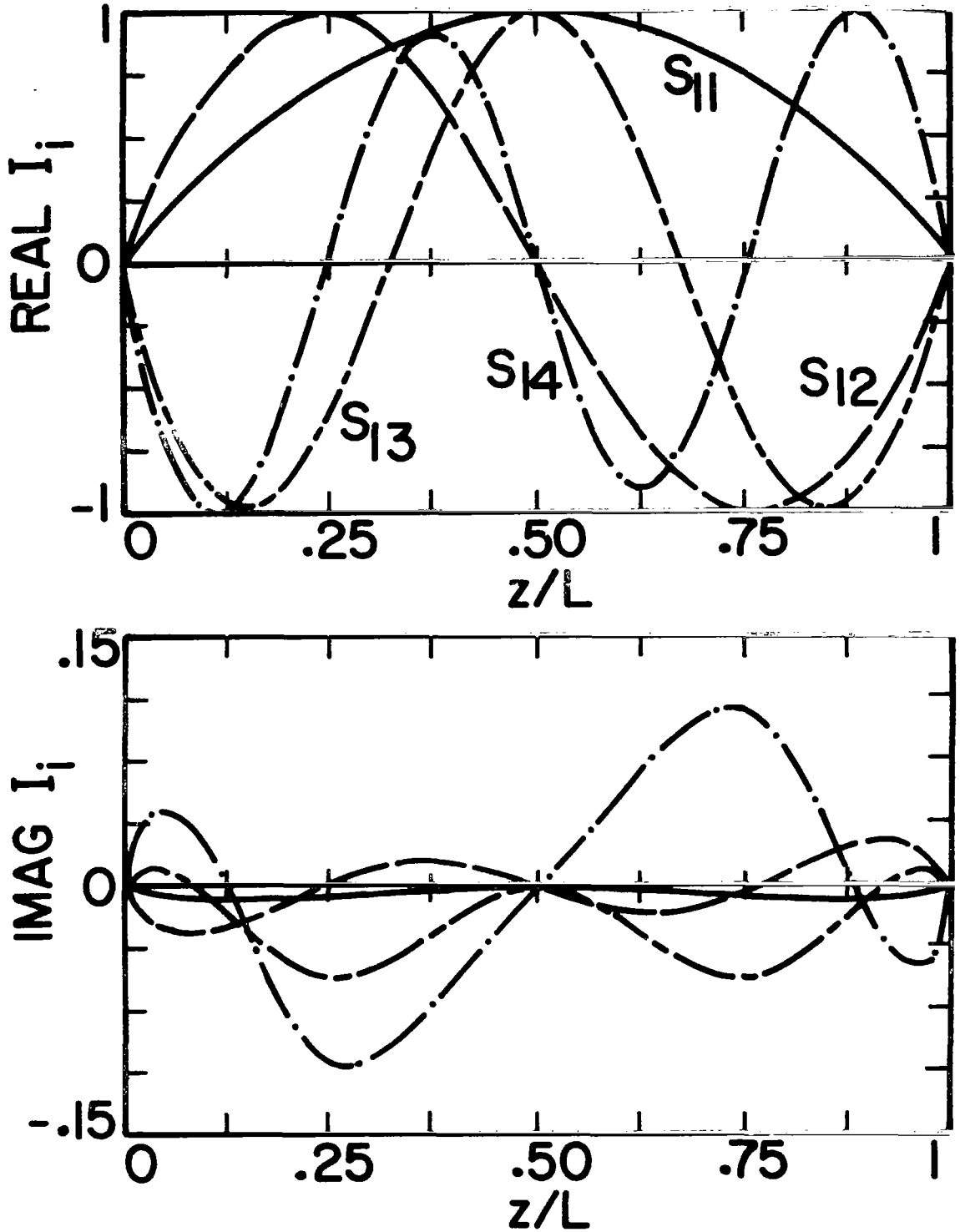

Figure 23. Current distribution of natural modes of circular cylinder over ground plane for resonant frequencies s_{11}, s_{12}, s_{13} and s_{14}, 2d/L = 1.0, 2a/L = 0.01.

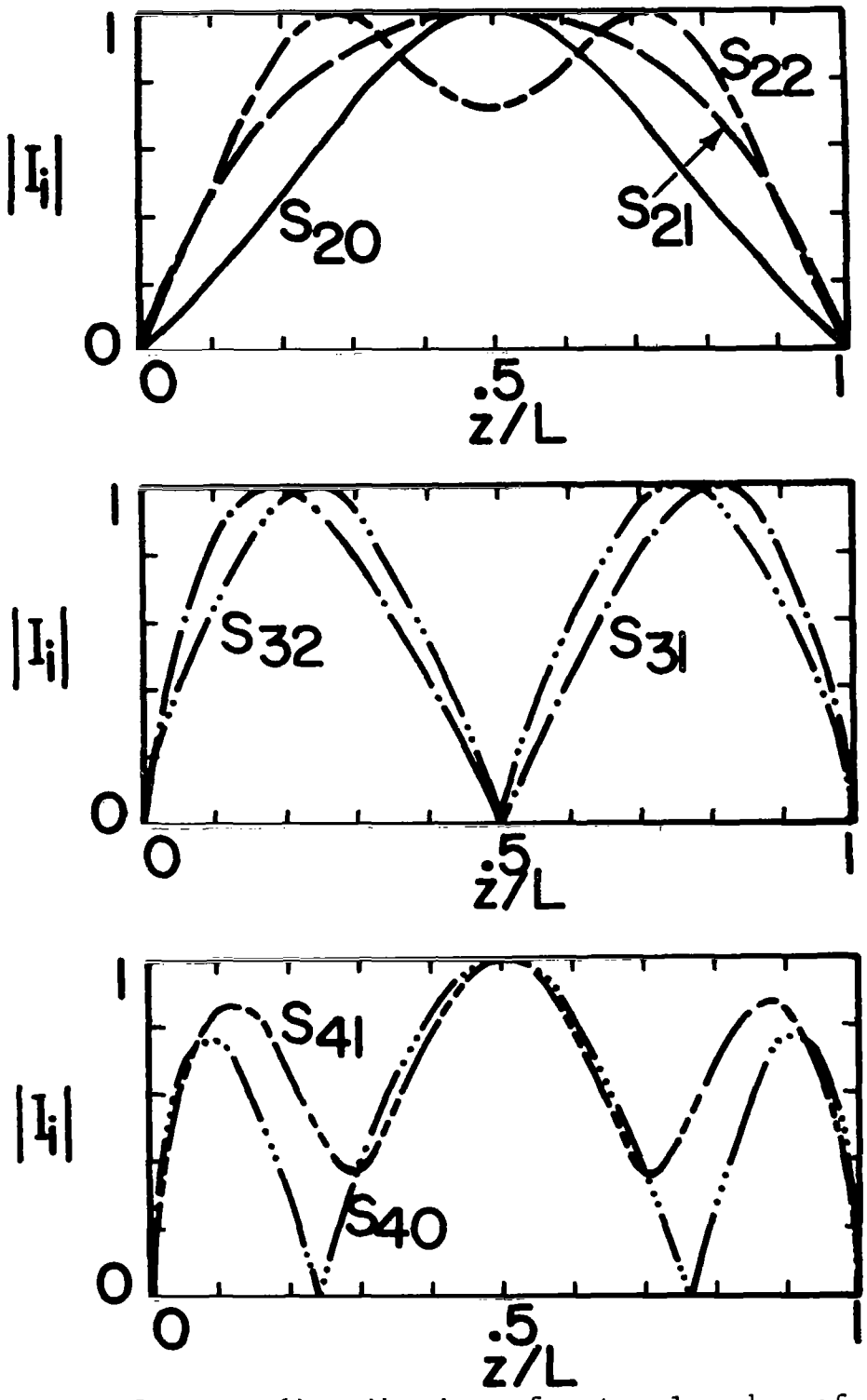

Figure 24. Current distribution of natural modes of circular cylinder over ground plane for second, third and fourth layer poles, 2d/L = 1.0, 2a/L = 0.01.

what the modal current distribution of the second and third poles, respectively, of the first layer.

The normalization constant $\beta_{\ell n}$ as defined in Equation (1.29) is calculated according to the procedure explained in Appendix B and in Figure 25 is shown the variation of β_{11} as the distance d above the ground is varied. β_{11} varies somewhat cyclically with respect to distance over the ground plane until the point is reached where the pole s_{11} leaves and a new pole enters the spiral path about the free space pole, at which point β_{11} changes phase and has a very large magnitude. The same variation in β_{22} is depicted in Figure 26 when the new pole s_{22} enters into the spiral path. Also, the variation of β_{23}, Figure 27, corresponding to pole s_{23}, is rather smooth along its trajectory until it too enters into the spiral path about the free space pole at a still larger distance above the ground plane.

According to Equation (1.32), the current response is proportional to the normalization constant $\beta_{\ell n}$. Figure 28 shows the current response in the frequency domain in the vicinity of the pole s_{11} at the center point of the structure due to a delta function plane wave normally incident. Neglecting the excitation due to the reflected field from the ground plane, the quantity of interest is

$$I(j\omega) = \sum_{\ell,n} \frac{\beta_{\ell n}}{j\omega - s_{\ell n}}$$

where the summation includes only the poles (and their complex

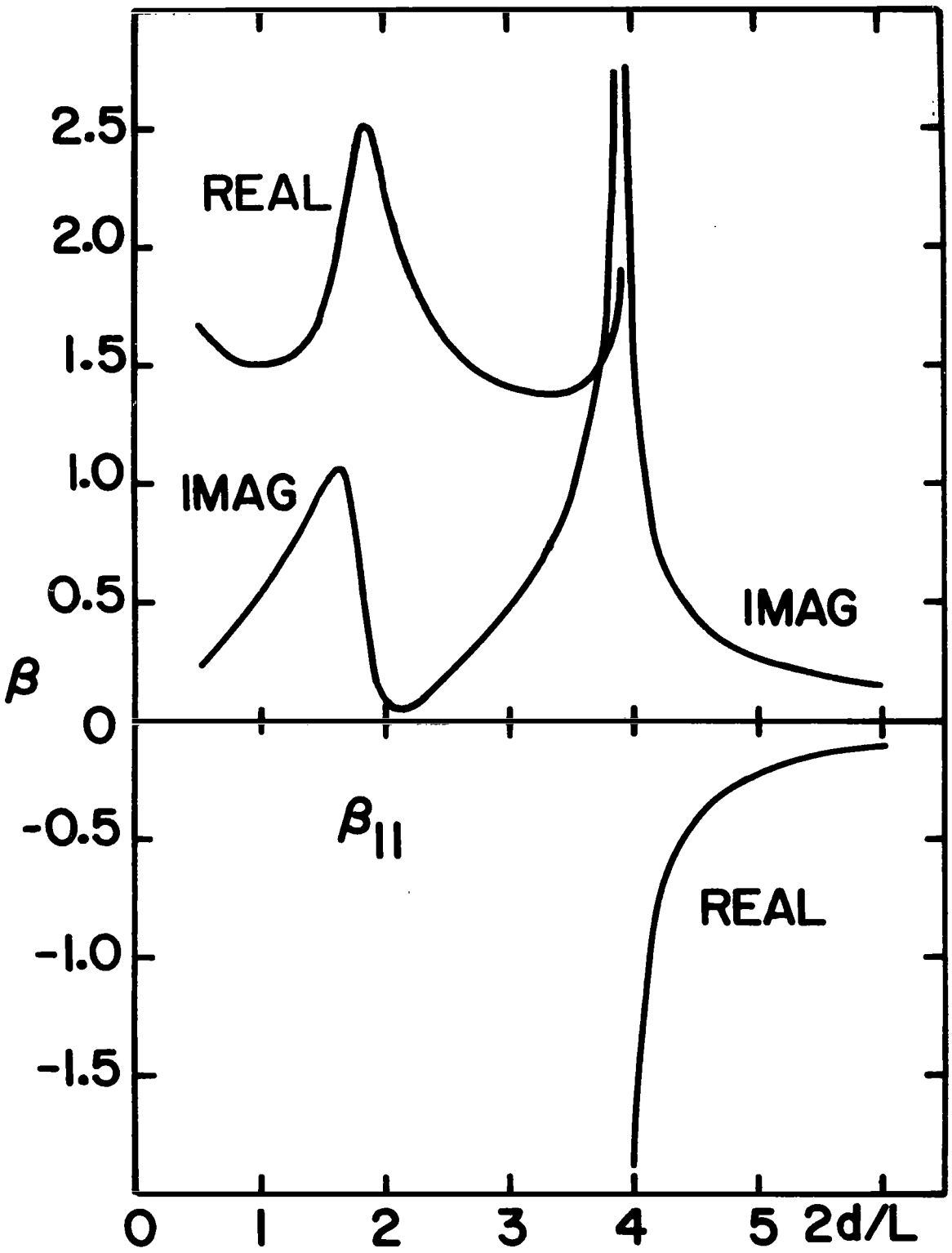

Figure 25. Normalization constant β_{11} as a function of distance over the ground plane, $2a/L = 0.01$.

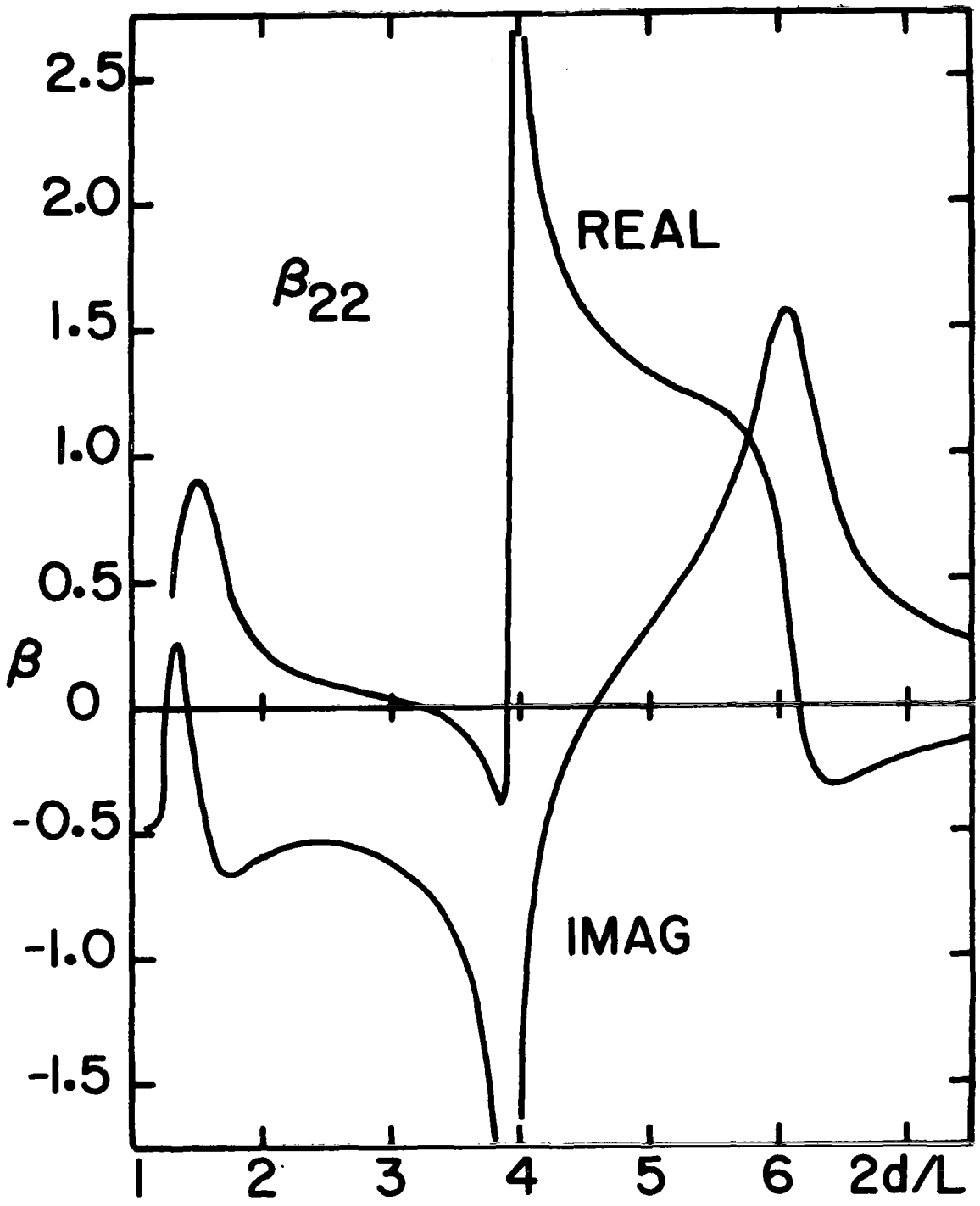

Figure 26. Normalization constant β_{22} as a function of distance over the ground plane, 2a/L = 0.01.

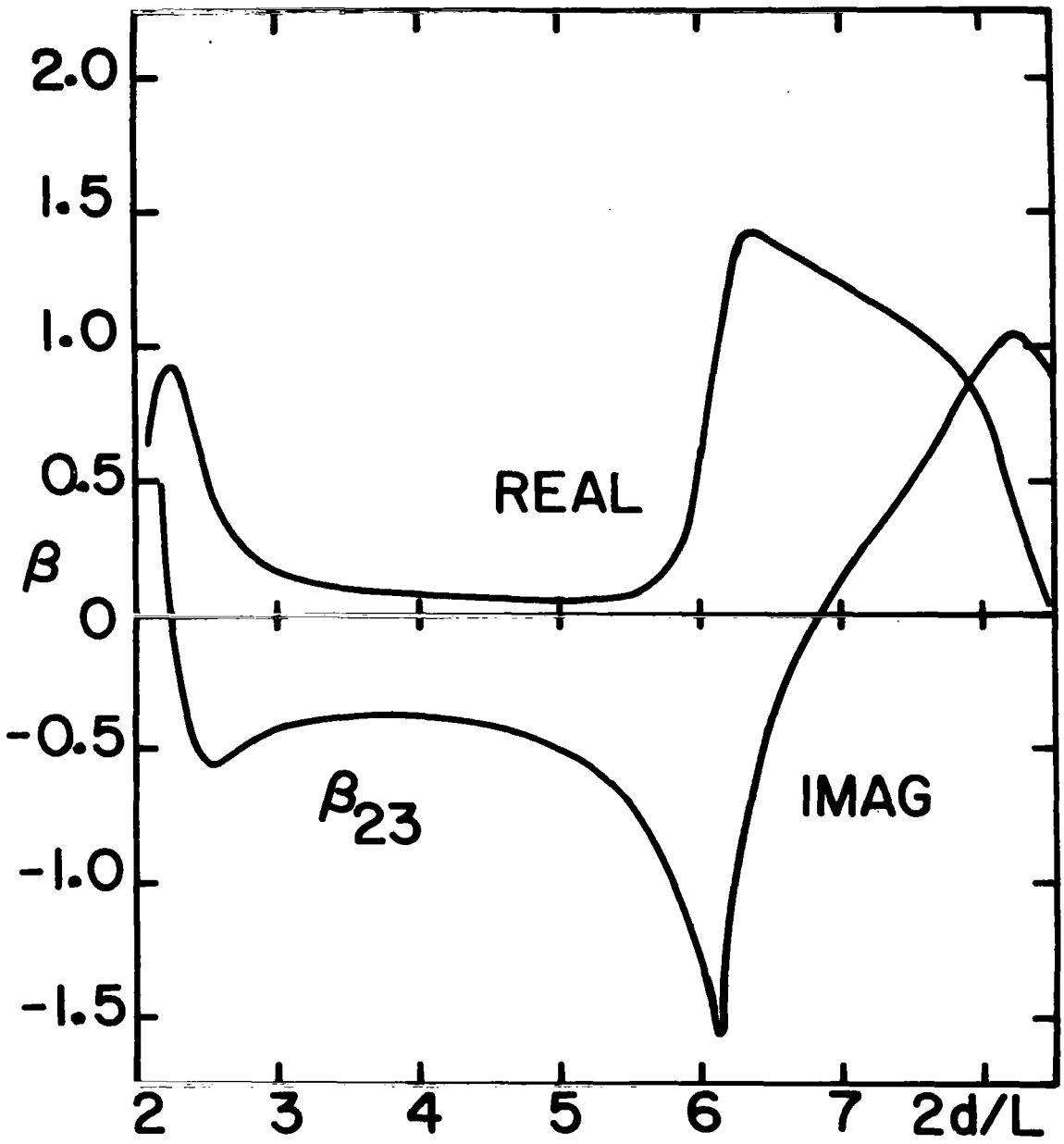

Figure 27. Normalization constant β_{23} as a function of distance over the ground plane, 2a/L = 0.01.

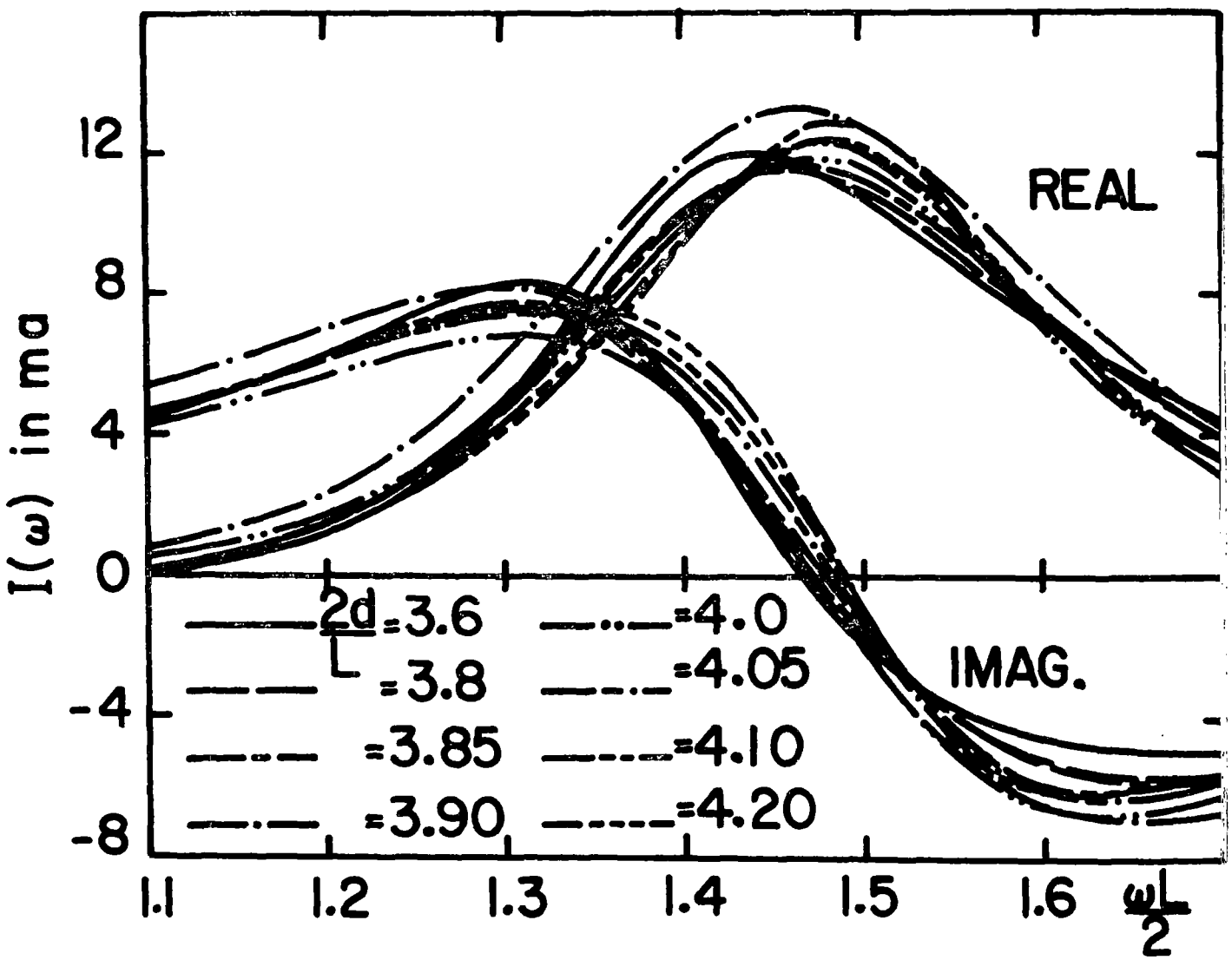

Figure 28. Variation of current as a function of frequency is the vicinity of pole s_{11}, $\theta = 30°$, $2d/L = 1.0$, $2a/L = 0.01$.

conjugates) s_{11} and s_{22}, which is on the verge of entering the spiral path of s_{11}. Even though the constants $\beta_{\ell n}$ vary abruptly in this region, their effect is smoothed somewhat on the $j\omega$-axis of the s-plane because of the tendency of the terms to cancel and because the denominator factor is largest in the same region. Hence, as one would intuitively expect, the magnitude of resonances in the frequency domain is not so strongly influenced by the distance of the wire above the ground as the spiral pole trajectories and the anomalous behavior of the $\beta_{\ell n}$ might suggest.

In Figure 29, the frequency domain current obtained from SEM calculations (Equation 1.32) at three points on the structure is given corresponding to a time harmonic plane wave incident and the results are compared at the center point of the circular cylinder by solving the integral equation by direct moment method solution in the frequency domain. The time domain current distribution is given in Figure 30, as obtained by SEM for E_θ-polarization with a step function plane wave incident and these results are checked at the center point by direct Fourier inversion of the frequency domain data obtained by solving the integral equation. The resultant time domain current at the center point of the structure obtained by the superposition of the incident and the reflected fields is shown in Figure 31. The figure clearly indicates the time delay involved in the reflected field due to the presence of the ground plane.

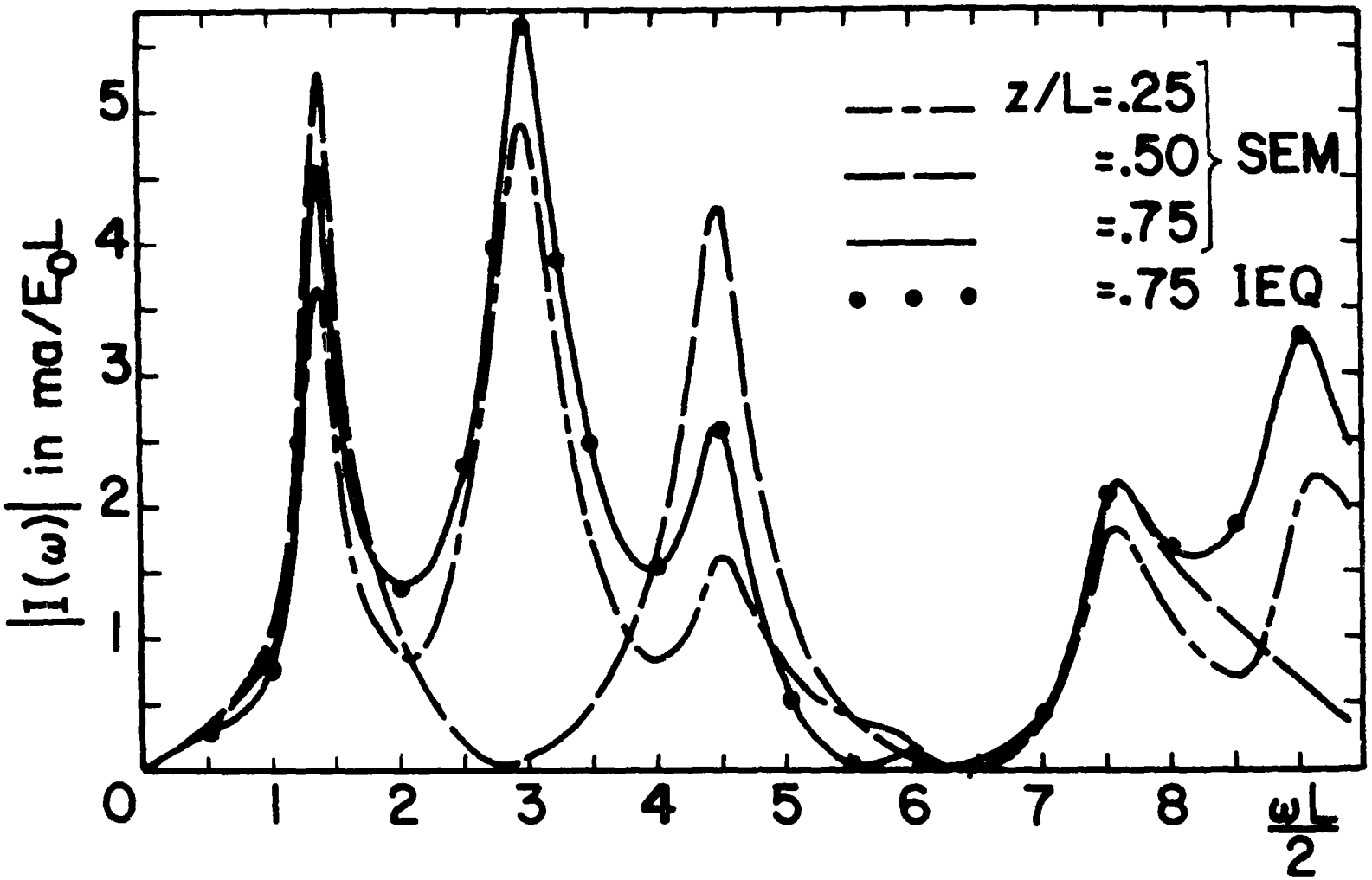

Figure 29. Variation of current on the circular cylinder over ground plane as a function of frequency for a plane wave incident, $\theta = 30°$, $2a/L = 0.01$.

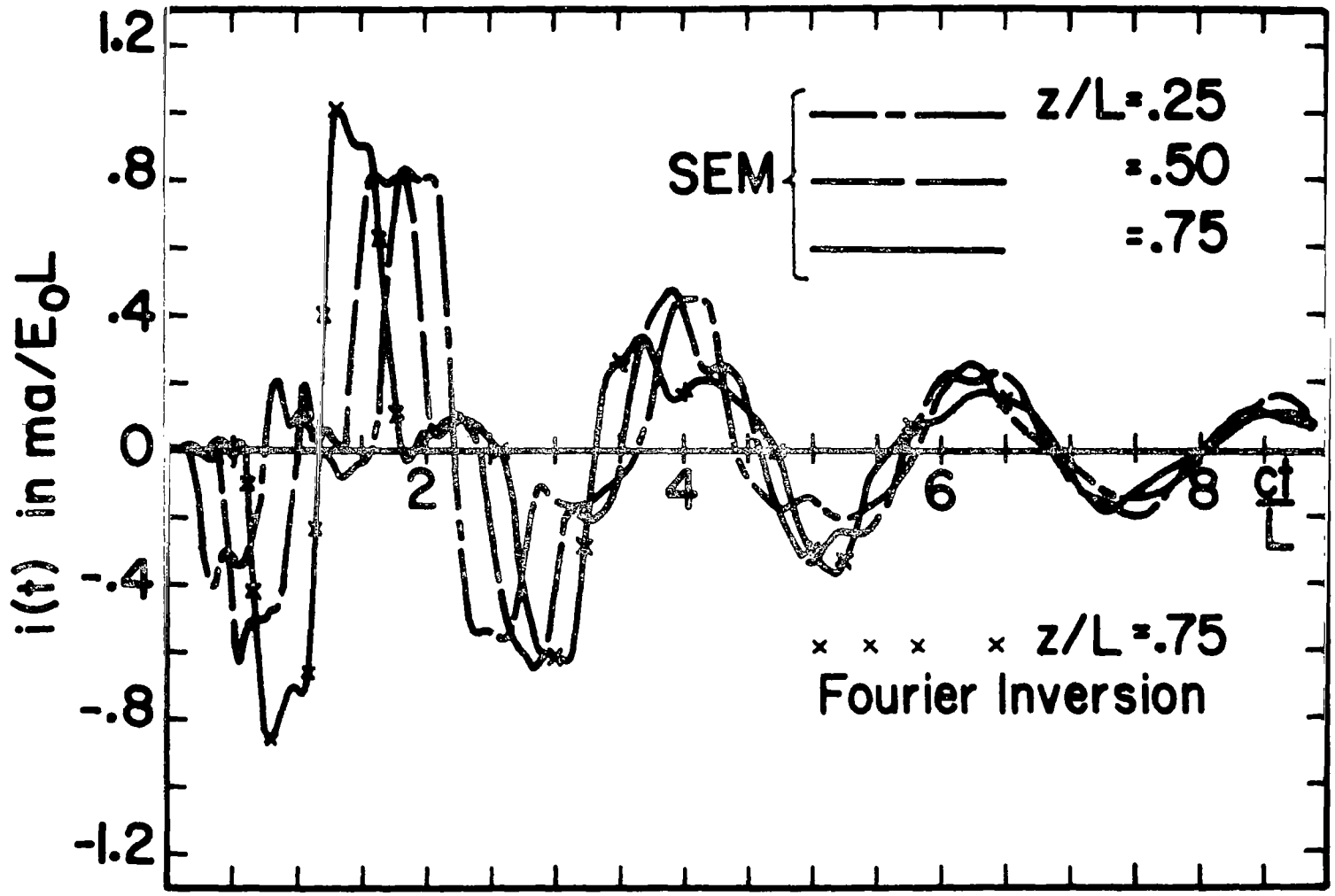

Figure 30. Time domain current, step function plane wave incident, $\theta = 30°$, $t = 0$ at $z = 0$, $2a/L = 0.01$.

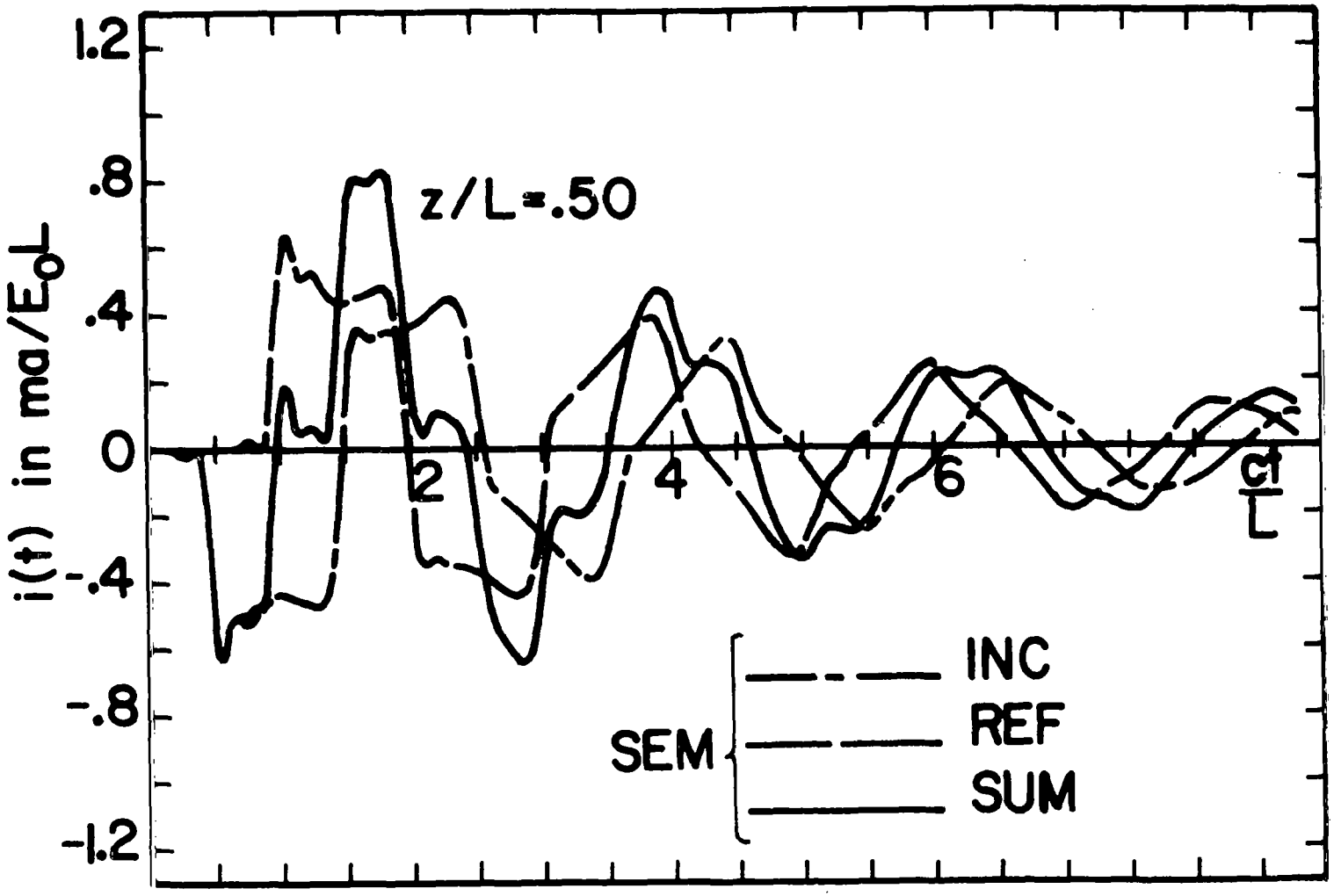

Figure 31. Time domain current, step function plane wave incident as the superposition of incident and reflected parts. $\theta = 30°$, $t = 0$ at $z = 0$, $2a/L = 0.01$.

Figure 32 shows the convergence of the time domain current as the number of poles closest to the $j\omega$-axis is increased.

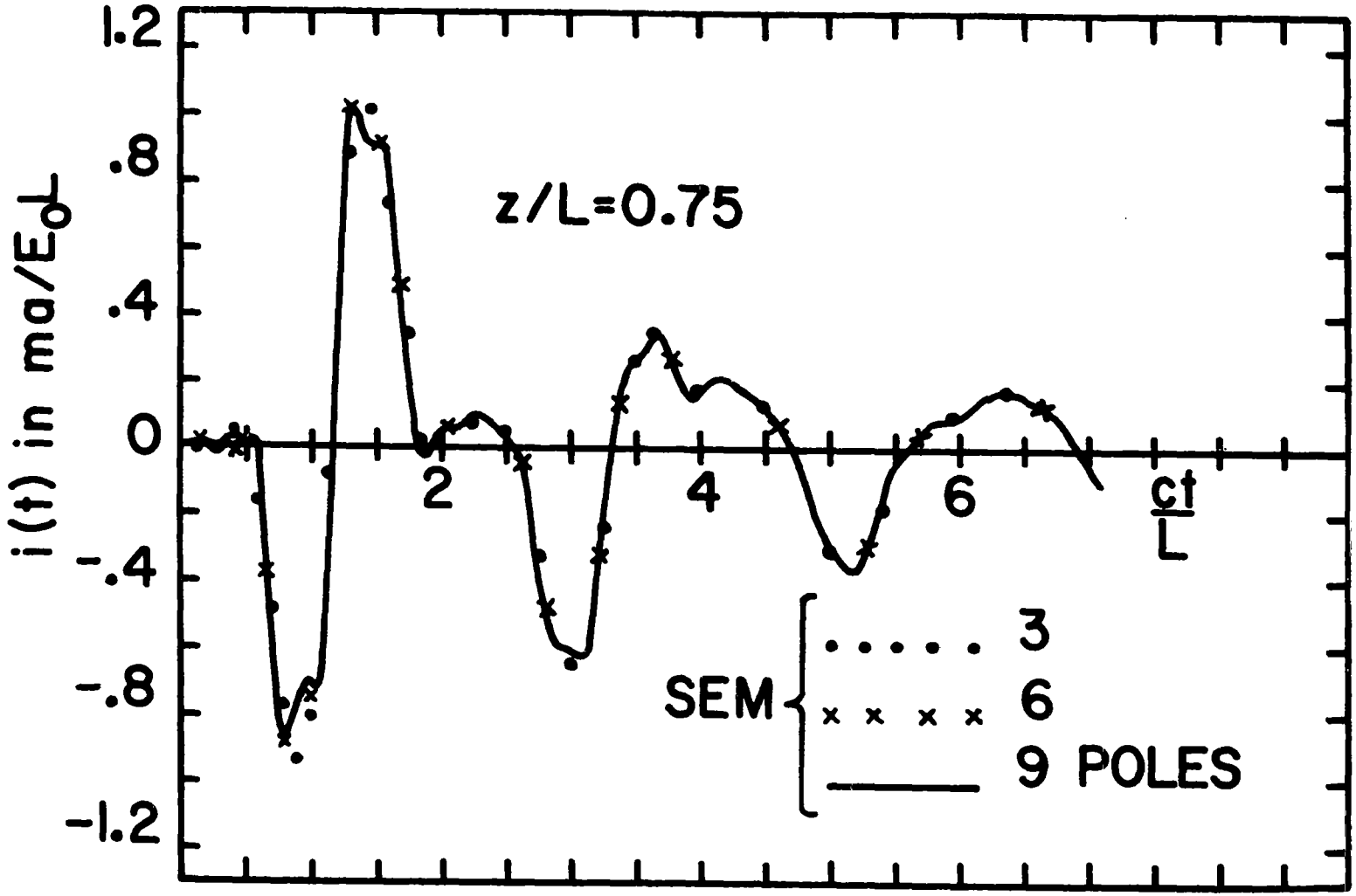

Figure 32. Convergence of time domain current, $\theta = 30°$, E_θ-polarization, step function plane wave incident, t = 0 at z = 0, 2a/L = 0.01, 2d/L = 1.0.

REFERENCES

[1] J.A. Stratton, Electromagnetic Theory, McGraw-Hill, New York, 1941.

[2] R.F. Harrington, Field Computation by Moment Methods, MacMillan, New York, 1968.

[3] F.M. Tesche, "On the Singularity Expansion Method as Applied to Electromagnetic Scattering from Thin-Wires," Interaction Note 102, April 1972.

[4] L.V. Kantorovich and V.I. Krylov, Approximate Methods of Higher Analysis, John Wiley and Sons, New York, 1959.

[5] C.M. Butler, Wire Antennas and Scatterers, Vol. 1, Department of Electrical Engineering, University of Mississippi, April, 1972.

[6] C.M. Butler, The Application of Moment Methods to Field Problems, Department of Electrical Engineering, University of Mississippi, May, 1973.

[7] C.D. Taylor and D.R. Wilton, "The Extended Boundary Condition Solution of the Dipole Antenna of Revolution," Interaction Note 113, June 1972.

[8] Wilton, D.R., and K.R. Umashankar, "Parametric study of an L-shaped wire using the singularity expansion method," Interaction Note 152, Air Force Weapons Laboratory, Albuquerque, NM, November, 1973.